HHS Public Access

Author manuscript

Sci Signal. Author manuscript; available in PMC 2022 September 09.

Published in final edited form as:

Sci Signal. ; 14(694): . doi:10.1126/scisignal.abe0387.

A genome-wide screen uncovers broad roles for mitochondrial nucleoside diphosphate kinases in inflammasome activation

Orna Ernst[1], **Jing Sun**[1], **Bin Lin**[1], **Balaji Banoth**[3], **Michael G. Dorrington**[1], **Jonathan Liang**[1,4], **Benjamin Schwarz**[6], **Kaitlin Stromberg**[6], **Samuel Katz**[1,4], **Sharat J. Vayttaden**[1], **Clinton J. Bradfield**[1], **Nadia Slepushkina**[2], **Christopher M. Rice**[5], **Eugen Buehler**[2], **Jaspal S. Khillan**[7], **Daniel W. McVicar**[5], **Catharine M. Bosio**[6], **Clare E. Bryant**[4], **Fayyaz S. Sutterwala**[3], **Scott Martin**[2], **Madhu Lal-Nag**[2], **Iain D.C. Fraser**[1,*]

[1]Signaling Systems Section, Laboratory of Immune System Biology, National Institute of Allergy and Infectious Diseases, NIH, Bethesda, MD, USA

[2]The Trans-NIH RNAi Facility, National Center for Advancing Translational Sciences, NIH, Rockville, MD, USA

[3]Department of Medicine, Cedars-Sinai Medical Center, Los-Angeles, CA, USA

[4]Department of Veterinary Medicine, University of Cambridge, Cambridge, CB3 0ES, UK

[5]Laboratory of Cancer Immunometabolism, National Cancer Institute, NIH, Frederick, MD, USA

[6]Laboratory of Bacteriology, National Institute of Allergy and Infectious Diseases, NIH, Hamilton, MT, USA

[7]Mouse Genetics and Gene Modification Section, Comparative Medicine Branch, National Institute of Allergy and Infectious Diseases, NIH, Bethesda, MD, USA.

Abstract

Non-canonical inflammasome activation by cytosolic LPS is a critical component of the host response to Gram-negative bacterial infection, however we lack a comprehensive understanding of the cellular processes that control this pathway. Using a genome-scale arrayed siRNA screen to discover inflammasome regulators in macrophages, we identified the mitochondrial *Nme4* gene, which codes for the multi-functional nucleoside diphosphate kinase D (NDPK-D), as a regulator of both non-canonical and canonical inflammasomes. We show that *Nme4* is required

[*]Address for correspondence: fraseri@nih.gov. **Contact for Materials and Resource Sharing** Further information and requests for reagents may be directed to, and will be fulfilled by the corresponding author, Dr. Iain D.C. Fraser (fraseri@niaid.nih.gov).

Author contributions

The study was conceived and designed by O.E., J.S., B.L. S.J.V., C.J.B., J.L. and I.D.C.F.; O.E. performed the majority of the experiments in this report and designed the CRISPR/Cas9 *Nme4*$^{-/-}$ mice; J.S. optimized the prime-trigger assay and generated the *Nme4*$^{-/-}$ RAW264.7 cells; B.L. optimized the RNAi delivery method and generated the *Traf6*$^{-/-}$ RAW264.7 cells; M.G.D. and O.E. performed the *in vivo* endotoxin shock experiments; B.B. performed the cardiolipin externalization experiments; J.L. generated the ASC-GFP expressing cells and measured ASC speck formation; S.J.V. and C.J.B. helped with image acquisition, visualization and analysis; C.M.R. helped with mitochondrial stress test experiments; N.S., E.B., S.M. and M.L-N. ran the genome-wide screen and analyzed the data; S.K. helped with genome-wide screen data analysis and mitochondrial localization analysis; B.S, K.A.S and C.M.B conducted the metabolomics analyses. J.S.K. generated the *Nme4*$^{-/-}$ mice; D.W.M., C.M.B., C.E.B., F.S.S., S.M., M.L-N. and I.D.C.F. supervised the project; O.E. and I.D.C.F. performed formal analysis of all data; O.E. and I.D.C.F. wrote the manuscript with input from all other authors.

Ethics declarations

The authors declare no competing interests.

for both mitochondrial DNA synthesis and cardiolipin exposure on the mitochondrial surface in response to priming signals, leading to broad inflammasome activation defects in *Nme4*-deficient cells. In addition, *Nme4* is required for TRAF6 mitochondrial recruitment and ROS production, which supports the large-scale TLR-induced gene program via *Nme4*-dependent TLR signaling responses. *Nme4* knock-out mice are protected from endotoxin-induced shock, consistent with attenuated ROS production and glycolytic commitment. Our findings suggest that in response to microbial challenge, *Nme4*-dependent TRAF6 mitochondrial recruitment triggers an energetic fitness checkpoint required to engage and support the transcriptional gene program necessary to support inflammasome activation.

Keywords

inflammasome; macrophage; LPS; IL-1; caspase-11; ROS

Introduction

Innate immune cells such as macrophages promote host defense by sensing pathogens via pattern recognition receptors (PRRs)[1]. While macrophages classically respond to lipopolysaccharide (LPS) from extracellular Gram-negative bacteria via Toll-like receptor (TLR)-4[2,3], more recent reports indicate intracellular detection of bacterial LPS relies on murine caspase-11 (caspases-4 and -5 in human cells) to induce pyroptosis and IL-1 release[4-7]. The host inflammatory response to such intracellular threats is mediated through multi-protein inflammasome complexes[8]. While several inflammasomes have been described to date[9-12], the canonical NLRP3 inflammasome has been the most heavily studied[13-21]. Minimally comprised of the NLRP3 sensor protein, the adaptor protein ASC, and caspase-1, it can be activated by a diverse array of stimuli including both pathogen and danger signals as well as a variety of cell stress inducers including ATP, Nigericin, crystal particles, reactive oxygen species (ROS) and oxidized mitochondrial DNA (mtDNA)[13,14,17,22]. Although a direct activating ligand has not been identified for NLRP3, canonical inflammasome activation invokes ASC oligomerization and caspase-1 activation and cleavage, which in turn cleaves the immature forms of the IL-1 family proteins and the recently identified pore-forming Gasdermin proteins[8,13,23-25].

The aforementioned cytosolic LPS sensing through caspase-11 is considered the non-canonical inflammasome pathway, as caspase-11 activation by LPS occurs upstream of NLRP3 activation[4]. Here, IL-1α maturation and secretion correlates with Gasdermin cleavage and pyroptosis that occurs independently from the poorly defined parallel activation of canonical NLRP3 and IL-1β release[4]. Two major checkpoints precede inflammasome activation by cytosolic LPS: an inflammatory priming signal, such as a TLR ligand, elevates the expression of key inflammasome genes while concomitant ‘licensing’ events post-translationally modify inflammasome components which may also be enriched at the mitochondrial outer membrane (MOM)[16,18,26]. It has been suggested that such recruitment is dependent on increased levels of the mitochondrial lipid cardiolipin at the MOM[18,20,26]. While numerous requirements for inflammasome activation have been

described, we still lack a comprehensive understanding of the cellular regulators of these critical inflammatory processes.

In addition to the observed recruitment of inflammasome effectors to the mitochondrial membrane, cellular metabolic pathways have been implicated in several aspects of inflammasome activation. During priming, PRR signaling induces succinate accumulation via TCA cycle disruption to support HIF1α-dependent *Il1b* transcription[27]. Mitochondrial ROS also contributes to activation of the canonical NLRP3 inflammasome[28,29]. It was recently reported that this ROS production is required for enhancing mtDNA synthesis through the mitochondrial nucleotide salvage pathway and that oxidized forms of this mtDNA released from the mitochondria can activate NLRP3[21]. Additionally, macrophage priming facilitates metabolic reprograming[30-33], known as glycolytic commitment, to elevate both aerobic glycolysis and glucose uptake and to reduce oxidative phosphorylation (OXPHOS) by rechanneling the electron transport chain (ETC) for ROS production[34]. Despite increasing insight into the critical role of mitochondrial responses and metabolic reprogramming during immune activation, how these events relate to and regulate the mitochondrial stress accompanying inflammasome activation is not clearly understood. Moreover, the relationship between the signaling and transcriptional events induced by PRR activation, and their relative impact on inflammasome priming and licensing, remain poorly defined.

In an effort to better describe the regulation of the non-canonical inflammasome, we conducted a genome-scale arrayed siRNA screen for regulators of IL-1α release in macrophages exposed to cytosolic LPS. We identified a requirement for nucleoside diphosphate kinases (NDPKs), the sole enzyme in the last step of the nucleoside salvage pathway in the mitochondria, and further elucidated the role of the *Nme4* gene (coding for NDPK-D, also known as NM23-H4) in inflammasome activation. We show that *Nme4* can regulate both canonical and non-canonical inflammasomes by supporting both cardiolipin enrichment on the MOM and mtDNA synthesis. We also find that *Nme4* is required for priming-induced ROS production to support PRR-activated TLR signaling and transcriptional responses. This novel role for *Nme4* and ROS in stimulus-dependent transcription is proportional to the scale of the gene program induced, and establishes a link between the macrophage metabolic capacity and the LPS-driven inflammatory response. Moreover, while *Nme4* is also required to support the glycolytic shift during macrophage activation, increased glycolysis is not required for the *Nme4* and ROS supported acute transcriptional responses. Our data help delineate the mitochondrial and metabolic processes critical for inflammasome activation and suggest that *Nme4* may coordinate a critical mitochondrial fitness checkpoint required to support a robust inflammasome response.

Results

A genome-wide siRNA screen identifies nucleoside diphosphate kinases as positive regulators of the non-canonical inflammasome

To discover regulators of the macrophage non-canonical inflammasome response to cytosolic bacteria, we first established a prime-trigger assay in which macrophages were treated with the TLR2 agonist, Pam3CSK4 (P3C), and then transfected with the

immunostimulatory component of LPS, Lipid-A. This assay induced comparable levels of IL-1α to those induced by the intracellular Gram-negative bacterium *Burkholderia cenocepacia,* both in the RAW264.7 mouse macrophage cell line and in primary mouse bone marrow-derived macrophages (BMDM) (Fig. 1 A, B). A GFP-expressing RAW264.7 cell line was employed[35], which permitted the development of a robust siRNA delivery protocol using GFP fluorescence reduction as a measure of transfection efficiency in 384-well format (Fig. S1A). When applied to the prime-trigger assay, delivery of *Casp4* siRNA (targeting mouse caspase-11) or *Il1a* siRNA strongly reduced the cytosolic LPS-driven release of IL-1α (Fig. 1C), but had no significant effect on TNFα secretion (Fig. S1B).

To identify regulators of the non-canonical inflammasome, a genome-wide arrayed siRNA screen was conducted. To mitigate siRNA seed-based off-target effects, we used three independent siRNAs/gene[36] and a screen-optimized Homogeneous Time-Resolved Fluorescence (HTRF) assay for IL-1α secretion (Fig. 1D). We identified numerous known pathway regulators among the strongest hits, including *Myd88* required for the TLR priming step, and *Casp4*, *Gsdmd* and *Il1a* required for cytosolic LPS detection and IL-1α release (Fig. 1E, Table S1). As expected, the canonical inflammasome regulators *Casp1* and *Nlrp3*, which should be dispensable for IL-1α release through the non-canonical pathway, did not show a screen phenotype (Fig. 1E). Analysis of a subset of signaling genes, targeting kinases, receptors and other cell signaling mediators, revealed a dependence on specific kinases in inflammasome activation (Fig 1F, Table S2). As expected, the kinases *Irak4* and *Irak2* were strong hits due to their requirement for the TLR2-dependent priming step in the screen assay (Fig. 1F, Table S2). Among the other genes positively regulating the non-canonical inflammasome response, we identified 3 members of the nucleoside diphosphate kinase (NDPK) *Nme* gene family, *Nme3, Nme4* and *Nme6* (Fig. 1F, Table S2). We noted that the products of each of these genes are the only NDPKs localized to mitochondria[37-39,40], which is considered an important cellular organelle in inflammasome activation[18-20,26]. Indeed, we could detect 92 genes that code for mitochondrial proteins in the top 5th percentile of screen hits (Fig. S2A, B, Table S3). In particular, *Nme4,* coding for the mitochondrial protein NDPK-D, has been previously implicated in a number of mitochondrial functions which could impact the inflammasome response[21,41-44].

Nme4/NDPK-D regulates the activation of both canonical and non-canonical inflammasomes

NDPK-D has been localized to both the mitochondrial intermembrane space and also to the matrix, where it has been shown to catalyze the last γ-phosphate transfer step in the mitochondrial nucleotide salvage pathway[38,44]. It has been recently proposed that the synthesis of new mitochondrial DNA (mtDNA), which requires this pathway as a nucleotide source, is a pre-requisite for the generation of TLR-induced oxidized-mtDNA, which in turn supports activation of the canonical NLRP3 inflammasome[21].

NDPK-D has also been shown to associate with the mitochondrial phospholipid cardiolipin, and facilitates its transfer between the mitochondrial inner- and outer membranes (MIM and MOM, respectively)[41]. Under resting conditions, cardiolipin localizes to the inner leaflet of the MIM, however mitochondrial stress can induce cardiolipin transfer to the

mitochondrial surface which enables release of stress signals such as cytochrome C[45]. Recently, cardiolipin exposure on the mitochondrial surface has been suggested to support canonical NLRP3 inflammasome activation through nucleation of a complex of key inflammasome regulators[18,26]. Taken together, these studies suggest that *Nme4*/NDPK-D could support inflammasome activation through both mitochondrial nucleotide synthesis and regulation of cardiolipin exposure.

To further investigate *Nme4* function, we first used CRISPR/Cas9 to target the *Nme4* gene in RAW264.7 cells (Fig. 2A), which recapitulated the initial non-canonical inflammasome screen IL1α phenotype in response to a P3C/transfected KLA prime-trigger stimulus (Fig. 2B). Since RAW264.7 cells do not express sufficient ASC to support canonical NLRP3 inflammasome activation, deficiencies in IL1α secretion are likely independent of the canonical inflammasome. To assess the role of *Nme4* in canonical inflammasome activation, we stably expressed ASC-GFP in wild-type and *Nme4*$^{-/-}$ RAW264.7 cells. Following cytosolic LPS (Fig. 2C), ATP or Nigericin (Fig. 2D) exposure, ASC-GFP expressing WT RAW264.7 cells support IL-1β and IL-1α release, whereas release of these cytokines is severely blunted in *Nme4*$^{-/-}$ cells, reinforcing a requirement for *Nme4* in both the canonical and non-canonical inflammasome pathways. We further used these cells to assess ASC speck formation, which indicates canonical inflammasome assembly, by dynamic live cell imaging, and observed markedly reduced ASC speck formation in the absence of *Nme4* (Fig. 2E, F, Movie S1), suggesting that *Nme4* is essential for effective formation of the NLRP3 inflammasome complex. The requirement for *Nme4* extended to the cellular pyroptotic response to cytosolic LPS, with Propidium Iodide (PI) uptake (Fig. 2G), LDH release (Fig S1C) and GSDMD cleavage (Fig 2H) all attenuated in *Nme4*$^{-/-}$ cells.

Nme4 is required for both cardiolipin exposure and LPS-induced mtDNA release

Since cardiolipin has been suggested to support non-transcriptional inflammasome licensing through recruitment of components to the mitochondrial membrane[26], and *Nme4* has been implicated in cardiolipin externalization[41,43], we hypothesized that this may contribute to defective inflammasome activation in *Nme4*-perturbed cells. We measured cardiolipin localization to the MOM and observed a substantially diminished LPS-induced increase in externalized cardiolipin in *Nme4*-deficient cells (Fig. 2I). A similarly defective response was observed when cardiolipin externalization was induced by the apoptotic stimulus staurosporine (Fig. 2I), implicating *Nme4* in multiple forms of mitochondrial stress-induced cell death, in agreement with previous studies showing *Nme4*-mediated cardiolipin exposure sensitizes cells to apoptosis[42] and mitophagy[43]. We also observed a marked reduction in the LPS-induced recruitment of NLRP3 to the MOM in *Nme4*-deficient cells (Fig. 2J), supporting a role for both *Nme4* and cardiolipin exposure in the mitochondrial events that embody inflammasome licensing. We further assessed the LPS-induced cytosolic release of mtDNA in macrophages, and observed a loss of this response in the absence of *Nme4* (Fig. 2K), in agreement with prior work[21,46]. These data support multiple roles for mitochondrial *Nme4* in canonical inflammasome activation.

Mitochondrial *Nme4* supports LPS-induced gene transcription

To further define the role of *Nme4* in the cellular processes supporting inflammasome activation, we measured the NF-κB and MAPK signaling responses that drive large-scale gene transcription programs in response to LPS priming. We measured the nuclear translocation of NF-κB (p65/RelA), degradation of the NF-κB inhibitor IκB, and phosphorylation of the MAPKs p38 and ERK1/2, and found *Nme4* deficiency resulted in diminished and delayed responses in all cases (Fig. 3A). We then tested IL-1α mRNA and protein expression and observed a diminished induction of *Il1a* in *Nme4*-deficient cells (Figs. 3B, C). Similarly weakened responses were observed for TNFα and IL-1β mRNA and protein (Fig. 3D, E, Fig. S3A), suggesting a broader role for *Nme4* beyond mtDNA synthesis and cardiolipin exposure. Considering the effects of *Nme4* deficiency on both LPS-induced signaling and inflammatory cytokine transcription, we tested the response of a wider gene panel to multiple TLR ligands, and found many inflammatory genes were broadly attenuated in the absence of *Nme4* (Fig. 3F, Table S4). Cluster analysis revealed two classes of genes: early transient genes, including *Dusp1* and *Rcan1*, for which expression was substantially delayed in the absence of *Nme4* (Fig. 3F, Fig S3B); and later sustained genes, including *Il6* and *Ccl3*, which were both delayed and diminished in the absence of *Nme4* (Fig. 3F, Fig. S3C). A similar delay was observed for inflammasome components which are induced during priming, including NLRP3 (Fig 3G, H) and caspase11 (Fig 3I, J). In contrast, the expression of constitutively-expressed inflammasome components not induced by priming, such as caspase1 and GSDMD, showed comparable expression levels in control and *Nme4*$^{-/-}$ cells (Fig. S3D, E). These observations suggest that *Nme4* is an important multi-functional regulator of mitochondrial events during macrophage activation, with an unexpected but critical role in LPS-induced transcription.

LPS-induced metabolic changes in macrophages are facilitated by *Nme4*

Since *Nme4* is a mitochondrial protein, we tested the metabolic characteristics of *Nme4*-deficient cells. Using a mitochondrial stress test, we observed a comparable basal oxygen consumption rate (OCR) in the absence of *Nme4* in both cell types, and detected the expected OCR reduction in response to LPS (Fig. 4A, B). The maximal respiratory capacity at the basal state was reduced in the *Nme4*-deficent cells, mainly due to the absence of respiratory reserve (Fig. 4B). Mitochondrial mass and membrane potential were not affected by *Nme4* deficiency (Fig. S4A-B). We found that the well-established increase in extracellular acidification rate (ECAR) from acute TLR-induced glycolysis, observable within minutes of an inflammatory signal[30,47,48], was markedly reduced in *Nme4*$^{-/-}$ macrophages (Fig. 4C). We then conducted a comprehensive metabolic profiling of WT and *Nme4*$^{-/-}$ macrophages (Fig. 4D) and noted a substantial difference in glycolytic and TCA metabolites (Fig. 4E). Furthermore, ADP accumulates in the *Nme4*$^{-/-}$ macrophages reflecting lower ATP levels in these cells. In the WT macrophages, TCA metabolites built up early on in response to LPS, suggesting a high energetic demand in response to LPS that is less evident in the *Nme4* deficient cells. The lack of glycolytic shift in the absence of *Nme4* is also reflected both by glucose accumulation and reduced flux in glycolysis intermediates compared to WT cells. Recent data have shown that the kinase TBK1 participates in the TLR-activated mitochondrial response that leads to the glycolytic shift[30,48], and consistent with a potential role for *Nme4* in this process, we observed reduced

TBK1 phosphorylation in *Nme4*-deficient cells (Fig. S4C). Considering the rapid glycolytic induction by LPS in control cells, we questioned whether glycolytic commitment is an energetic pre-requisite for the robust transcriptional response. While we observed normal induction of numerous inflammatory cytokine mRNAs (Fig. 4F) in macrophages treated with the glycolysis inhibitor 2-DG (Fig. S4D), the later sustained transcription of *Il1a* and *Il1b* was reduced (Fig. 4G), consistent with prior observations[27,49]. Similarly, sustained secretion of TNFα, which requires glycolysis-dependent metabolic reprogramming[27,30], is strongly diminished in the presence of 2-DG (Fig. 4H). Thus, while the defective glycolysis induction we observe in *Nme4*-deficient macrophages may limit their energetic capacity to support a sustained inflammatory state, it does not explain their early diminished transcriptional response to LPS.

Nme4 is required for mitochondrial recruitment of TRAF6 and ROS production in response to LPS

It has been shown that activated macrophages utilize the electron transport chain for the production of reaction oxygen species (ROS) which are a critical component of the host antibacterial response[30,50]. We measured the early ROS response to LPS and observed a ROS induction deficiency in the absence of *Nme4*, both at the population (Fig. 5A) and single cell level (Fig. 5B). Mitochondrial ROS can be generated either via OXPHOS complexes I and III or through reverse electron flow in the ETC which reduces mitochondrial membrane potential in response to LPS[33,34], while the macrophage inflammatory response has been shown to be driven by mitochondrial ROS produced specifically in complex III[33]. The dampened mitochondrial ROS in the *Nme4*-deficient cells is consistent with our observed reduction in TCA metabolites in these cells (Fig. 4E). Accordingly, we saw progressively reduced mitochondrial membrane potential in LPS treated macrophages which was both delayed and diminished in *Nme4*$^{-/-}$ cells (Fig. 5C), consistent with the lack of early ROS production in the absence of *Nme4*. Since it has been suggested that antioxidants can diminish LPS-induced inflammatory gene activation[50-52], we tested whether mitochondrial ROS induction contributes to the early transcriptional response. We find that inhibition of mitochondrial ROS with the scavenger mitoTEMPO perturbs LPS-induced gene responses (Fig. 5D), and we observe a similar effect with the antioxidant N-acetylcysteine (NAC, Fig. S5A). These data support a model whereby defective ROS production underlies the acute transcriptional defect in LPS-treated *Nme4*$^{-/-}$ cells.

By assessing early ROS induction by LPS in the presence or absence of 2-DG, we found that glycolysis inhibition had no significant effect on the early production of ROS (Fig. 5F) whereas ROS inhibition markedly reduced acute glycolytic commitment induced by LPS (Fig. 5G) suggesting that ROS production precedes the glycolytic shift. Accordingly, *Nme4*$^{-/-}$ cells fail to induce both ROS (Fig. 5A, B) and increases in glycolytic flux (Fig. 4C). These data indicate that *Nme4* likely operates upstream of the mitochondrial ROS production that dictates the glycolytic shift and sustained transcription of *Il1a* and *Il1b*.

It has been suggested that TRAF6 recruitment to the MOM is required both for ROS production[50] and glycolytic commitment[48] in LPS-treated macrophages. Therefore we

sought to determine whether TRAF6 is responsible for signaling to the mitochondria to engage *Nme4* after LPS treatment. We detected substantial increases in TRAF6 in the mitochondrial fraction of LPS-treated wild type macrophages, while *Nme4*$^{-/-}$ cells showed lower basal levels of TRAF6 in the mitochondrial fraction and no LPS-induced increase (Fig. 5H). We measured TRAF6 translocation in the presence of a ROS inhibitor and observed no decrease in LPS-induced recruitment (Fig. S5B), suggesting that TRAF6 movement to the MOM is upstream of ROS production, as previously reported[50]. We then used CRISPR/Cas9 to generate *Traf6*$^{-/-}$ RAW264.7 cells and, similar to *Nme4*$^{-/-}$ macrophages, we find that these cells cannot induce an early ROS response (Fig. 5I) or a glycolytic shift after LPS treatment (Fig. 5J). Taken together, these data suggest that a mitochondrial ROS response is critical to support the acute LPS-activated gene program and is *Nme4*-dependent. We find that *Nme4* is required for this ROS response, possibly through facilitation of TRAF6 MOM recruitment which may depend on the *Nme4*-supported cardiolipin enrichment on the mitochondrial surface.

Nme4 coordinates a metabolic checkpoint to support a robust cellular response to infection

Considering that the LPS-induced gene program is severely hampered in *Nme4* depleted cells, we hypothesized that *Nme4*-dependent mitochondrial responses may be required to initiate and support large-scale transcription in TLR-activated macrophages. To test whether the effects of *Nme4* deficiency on transcription are scale dependent, we compared LPS-activated macrophages with those stimulated with either IFN-γ or PGE_2, which induce substantially fewer genes (Fig. S6A, B)[53]. We chose a panel of 10 genes for which at least half were induced by each ligand, with several genes induced by all three. We found that all genes induced by LPS were substantially attenuated in the *Nme4*$^{-/-}$ cells, approximately half of the IFN-γ induced genes were perturbed, while all PGE_2-induced genes were expressed to similar levels in control and *Nme4*$^{-/-}$ cells (Fig. 6A). These data support a model whereby the larger energetic demands placed on the cell to induce numerous genes in response to LPS likely require mitochondrial responses dependent on nucleoside diphosphate kinases.

Mice lacking *Nme4* are resistant to endotoxin shock.

We used CRISPR/Cas9 to target the *Nme4* gene locus (Fig. S7A) and generated *Nme4*$^{-/-}$ mice which appeared healthy and showed Mendelian inheritance. We tested the response of *Nme4*$^{-/-}$ mice to endotoxin-induced sepsis and observed significant resistance to septic shock in the *Nme4*$^{-/-}$ animals (Fig. 6B). Unexpectedly, we observed a normal IL-1α response to cytosolic LPS in BMDM from these mice (Fig. S7B). However, we could replicate the *Nme4* dependency of the IL-1α/β responses to cytosolic LPS in BMDM when the gene was acutely perturbed by three independent siRNAs (Fig. S7C, D). We therefore hypothesized that other *Nme* gene family members might compensate for the loss of *Nme4 in vivo*. When we individually knocked down the other two *Nme* genes, *Nme3* and *Nme6*, that were identified in our initial screen, we observed diminished IL-1α and IL-1β responses to cytosolic LPS in primary BMDMs (Fig. S7E, F), especially in the *Nme6*-perturbed cells. Thus, *Nme3* and *Nme6* also contribute to the cytosolic LPS response in primary macrophages, and likely compensate for *Nme4* deficiency *in vivo*. Accordingly,

we observed elevated levels of both *Nme3* and *Nme6* in the *Nme4*$^{-/-}$ BMDM (Fig S7G, H). Consistent with this, we found that *Nme4*$^{-/-}$ BMDM were more sensitive than WT BMDM to siRNA-mediated knockdown of either *Nme3* or *Nme6* (Fig. 6C). Moreover, combined knockdown of both *Nme3* and *Nme6* in BMDM from *Nme4*$^{-/-}$ mice reduced IL-1α to levels comparable with *Casp4*-depleted cells (Fig. 6C). As was observed for the *Nme4*$^{-/-}$ RAW264.7 cells, *Il1b* expression and ROS production were reduced when both *Nme3* and *Nme6* were knocked down in *Nme4*$^{-/-}$ BMDM (Fig. 6D) suggesting that inflammasome priming is defective in the absence of the mitochondrial *Nme* genes.

Since the *Nme4*$^{-/-}$ mice exhibit a normal IL-1α response to cytosolic LPS, the protective effect of *Nme4* perturbation for *in vivo* endotoxin challenge might relate to the other mitochondrial functions for *Nme4* observed in our earlier experiments and in prior studies[54-56], including a role for *Nme4* in mitophagy[43]. Accordingly, we found that resistance to endotoxin was also observed in mice pre-injected with the ROS scavenger N-acetyl cysteine (NAC) (Fig. 6E), supporting a role for ROS in promoting broader aspects of the inflammatory lethality of LPS *in vivo*. We also observed a defective glycolytic commitment in the *Nme4*$^{-/-}$ BMDM, both in the acute response to LPS (Fig. 6F) and at 24 hour after LPS stimulation (Fig. 6G). This defective glycolytic commitment in macrophages from *Nme4*$^{-/-}$ mice may also contribute to their endotoxin resistance, as glycolytic blockage by 2-DG has a similarly protective effect in this LPS challenge model[57-59].

Discussion

We have utilized a genome-scale siRNA screening approach to discover new regulators of inflammasome activation, identifying the three mitochondrial proteins of the *Nme* gene family as novel regulators of the non-canonical inflammasome. We focused on the *Nme4* gene, as it codes for a multifunctional protein (NDPK-D) that could be linked to the canonical inflammasome response through both MOM cardiolipin enrichment[18,26,41] and mitochondrial DNA synthesis[21,44]. In this work we have further illuminated *Nme4's* roles in these processes, while also uncovering unappreciated functions of *Nme4* in both canonical and non-canonical inflammasome responses. We demonstrate that *Nme4* is required for cardiolipin exposure on the MOM in response to a TLR priming signal, which in turn may support the recruitment of inflammasome components to the MOM during inflammasome licensing. We confirm that *Nme4* is required for TLR-induced mtDNA synthesis, but also delineate additional roles for *Nme4* in mitochondrial recruitment of TRAF6 and ROS production, which are required for the large-scale inflammatory gene program induced during inflammasome priming.

While the known role for *Nme4* in the mtDNA salvage pathway depends on its nucleoside diphosphate kinase function in the final step of NTP synthesis, its cardiolipin transferase activity highlights reciprocally regulated dual functions, as cardiolipin binding inhibits NDPK-D kinase activity due to the close proximity between the lipid binding pocket and the catalytic domain[42]. Notably, other *Nme* genes exhibit a similar multi-functional nature, with *Nme1* and *Nme2* recently implicated as protein histidine kinases[60], *Nme1* regulating non-homologous end joining of DNA double-strand breaks[61], *Nme3* being critical for mitochondrial fusion[37], and *Nme6* and *Nme7* regulating stem cell gene expression[62]. Further

studies will be required to determine whether the additional role we have identified for *Nme4* in TRAF6 MOM recruitment, ROS production and gene transcription is dependent on its kinase or lipid transferase function, or yet another unappreciated activity for its NDPK-D gene product.

Although our screen was initially designed to identify regulators of the non-canonical inflammasome, restoration of the canonical inflammasome by ASC expression in RAW264.7 macrophages demonstrated a requirement for *Nme4* in both pathways, and our unexpected finding that *Nme4* is also broadly required for transcriptional priming has obvious implications for multiple inflammasome classes. We show that *Nme4* deficiency leads to a delay in both TLR-induced signaling and acute gene transcription, and a defective metabolic shift, implying that mitochondrial engagement is an early event in TLR pathway activation, consistent with recent observations[47].

Mitochondria subsume a central role in the macrophage response to infection where they dictate major metabolic changes that direct ATP production from OXPHOS to aerobic glycolysis. This switch is accompanied by alteration of TCA cycle flux, including the accumulation of TCA metabolites and increased ROS production[51,63]. While the glycolytic commitment in TLR-activated macrophages is well established[30,32,47,48,64], studies with 2DG-based glycolysis blocking have shown that the majority of TLR-induced genes are not dependent on this metabolic switch[27,30,65]. The primary exception to this pattern is IL-1β, whose TLR-activated transcription has been linked directly to the aforementioned TCA cycle flux alteration that increases succinate levels and activates HIF-1α through protein stabilization, which in turn directly upregulates the *Il1b* gene[27,31,57]. While we demonstrate that the acute glycolytic response is defective in *Nme4*-deficient macrophages, this cannot explain the broad and acute TLR-induced gene expression defect in these cells that is evident 1-2 hr after ligand activation.

Rather, our study finds that acute *Nme4*-dependent ROS elevation in macrophages is critical to support this early gene transcription. This ROS response requires mitochondrial recruitment of TRAF6, which is also defective in *Nme4*-deficient cells. Prior work has suggested that MAVS is required for TRAF6 MOM enrichment, however we observe no change in MAVS levels on the mitochondria in the absence of *Nme4* (data not shown). Therefore, the *Nme4*-dependent loss of cardiolipin MOM enrichment may suggest that this lipid also contributes to the TRAF6 recruitment. Since we find that NF-κB and MAPK signaling are reduced and delayed in the *Nme4*-deficient cells, this suggests that TRAF6 recruitment to the mitochondria is required for intact TLR signaling responses and robust early gene transcription.

The requirement for ROS activation to support TLR-induced transcription is supported by the attenuation of cytokine genes by the mitochondrial ROS scavenger mitoTempo, and the general ROS scavenger NAC. ROS can be produced in macrophages via diverse sources in several cellular locations and time frames. In addition to respiration-induced ROS in the mitochondria[66], ROS can also be generated as part of the pentose phosphate pathway by NADPH oxidase (NOX)[66], and as a byproduct of fatty acid and protein oxidation at the ER[66]. It has been shown that NF-κB activity is dependent on NOX expression[67] and is

elevated during hydrogen peroxidase-induced oxidative stress[68]. Our data suggest a role for *Nme*-dependent mitochondrial ROS, which is critical for acute NF-κB signaling to support TLR-activated gene transcription.

Nme4$^{-/-}$ mice are protected from LPS shock, although *Nme4*$^{-/-}$ BMDM did not exhibit an *in vitro* IL-1α secretion defect in response to cytosolic LPS. It would appear that *Nme4*'s support of non-canonical inflammasome activation can be compensated by the other *Nme* genes identified in our initial screen, *Nme3* and *Nme6*, as their perturbation in *Nme4*$^{-/-}$ BMDM uncovered both the IL-1α secretion and ROS response defect resulting from *Nme* deficiency. BMDM from *Nme4*$^{-/-}$ mice did however exhibit a strong defect in glycolytic commitment in response to LPS, which may contribute to their protection from endotoxin shock, and would be consistent with recent studies showing a similar protective outcome in mice treated with the glycolysis inhibitor 2DG[57-59]. Also, while 2DG does not block inflammatory cytokine transcription beyond the succinate/HIF-1α/IL-1β axis, it does have substantial effects on sustained secretion of inflammatory cytokine proteins[27,57,69], which would be consistent with reduced susceptibility to LPS-induced shock in mice with a perturbed glycolytic commitment pathway. *Nme4* has also been shown to regulate mitochondrial turnover through mitophagy[43], a process also implicated in the macrophage response to infection[70,71], however, we did not observe elevated mitochondrial mass in *Nme4*$^{-/-}$ cells.

In summary, we have identified the *Nme4* gene as a multifunctional regulator of inflammasome activation based on multiple mitochondrial roles for its NDPK-D protein product (Fig. 7). We show that *Nme4* coordinates TLR-induced mtDNA synthesis and cardiolipin MOM exposure, which supports mitochondrial nucleation of inflammasome components. *Nme4* also facilitates TRAF6 mitochondrial recruitment, supporting both ROS induction and glycolytic commitment, with the former effect on ROS being required for initiating and supporting both TLR-induced NF-κB and MAPK signaling, and the broad transcriptional program which underpins inflammasome priming. Our work suggests that *Nme4*-sufficiency can function as a mitochondrial fitness checkpoint which can determine the capacity of macrophage cells to support a robust metabolic and transcriptional response to infectious challenge.

Methods

1. Reagents

Lipid A (Avanti Polar Lipids), Pam3CSK4, R848, nigericin and ATP (InvivoGen), LPS, NAC, mitoTempo, 2DG, oligomycin, FCCP, Rotenone, antimycin A, TMRM, FCCP, PGE_2, Tributylamine were from Sigma-Aldrich. MitoTracker Green, Hoechst 33342 (ThermoFisher), LCMS-grade water, methanol, isopropanol, chloroform and acetic acid (Fisher Scientific), IFNγ (PeproTech), ELISA kits (IL-1α, IL-1β, TNFα from R&D).

2. Cell Lines

RAW264.7 (ATCC), RAW264.7 G9 cells were derived from an authenticated batch of RAW264.7 cells used by the Alliance for Cell signaling consortium[35]. RAW264.7 cells

were maintained in complete DMEM media, comprising DMEM with 4.5 g/L glucose, 10% FBS (Gemini Bio-Products, West Sacramento, CA), 2 mM Glutamine (Lonza) and 20 mM HEPES (Lonza), hereafter complete DMEM.

3. Generation of CRISPR/Cas9-based gene edited cell lines

gRNAs targeting mouse *Nme4* or *Traf6* were designed using the Zhang lab online tool (https://zlab.bio/guide-design-resources) and cloned into the pX330-U6-Chimeric_BB-CBh-hSpCas9 plasmid (Addgene #42230)[72]. Plasmids were electroporated into RAW264.7 cells in the presence of a GFP expressing vector (Amaxa). 16 hr later, GFP+ cells were sorted into single cells clones. Clone knockout was confirmed by genomic DNA extraction (Qiagen), gene amplification and sequencing. gRNA sequences used: g*Nme4*#1 targeting exon 1: CAGCCTTTTCGGGCGCGTCG; g*Nme4*#2 targeting exon 2: ATACAACGCTTTGAGAGGCG; g*Traf6*: GAAGCAGTGCAAACACCATG.

4. Generation of ASC-GFP RAW264.7 cell lines

The lentiviral plasmid pLEX-MCS-ASC-GFP (Addgene #73957) and packaging plasmids pCMV-VSV-G (Addgene #8454) and pCMV-delta-R8.2 (Addgene #12263) were transfected into adherent HEK293T17 cells using the TransIT-Lenti transfection system (Mirus). 72 hr later, supernatant was collected, and virus was concentrated using Lenti-X Concentrator (Takara). WT and *Nme4*$^{-/-}$ RAW264.7 cells were transduced with concentrated lentivirus for 72 hrs, and subjected to puromycin (2 μg/ml) selection for >10 days. WT RAW264.7 ASC-GFP and *Nme4*$^{-/-}$ ASC-GFP monoclonal cell lines were isolated by a limiting dilution and the clones used in this study were selected based on moderate ASC-GFP fluorescent signal and lack of spontaneous ASC speck formation in the absence of inflammasome priming and triggering stimuli.

5. Mice and generation of CRISPR/Cas9 Nme4$^{-/-}$ strain

All mice were maintained in specific pathogen-free facilities under 12 hr light dark cycles with access to food and water ad libitum. All procedures were approved by the National Institute of Allergy and Infectious Diseases Animal Care and Use Committee (National Institutes of Health, Bethesda, MD). C57BL/6 were obtained from Jackson Laboratories. *Nme4*$^{-/-}$ mice were generated on the background of C57BL/6 using the two gRNAs described above to achieve a 248 bp deletion in the *Nme4* loci, which codes for a frame shifted protein. Three to 4-week-old C57BL/6 female mice from Taconic Labs were superovulated by IP injection of 5 IU of pregnant mare serum gonadotropin (Prospec Protein Specialists) followed 48 hr later by 5IU of human chorionic gonadotropin (Sigma Aldrich). The females were then mated with the C57BL6 males and one cell embryos were isolated from the pregnant females. The embryos were then microinjected into pronuclei with a mixture of Cas9 (10 ng/ul) obtained from IDT and sgRNA (10 ng/ul) from Thermofisher. The microinjected embryos were transferred into oviducts of CD1 pseudo-pregnant mothers. The pups were weaned at three weeks and the ear punch biopsies were genotyped for the mutation by PCR and sequencing. Muscle tissue from the mouse femur was used to extract mitochondria which were blotted for *Nme4* (the antibody was a kind gift from Dr. Marie-Lise Lacombe). Mouse BMDM were prepared by differentiation from bone marrow

for 7 days in complete DMEM supplemented with 100 U/ml Penicillin-Streptomycin and 50 ng/ml M-CSF (R&D).

6. Endotoxin shock

Female WT or *Nme4*$^{-/-}$ mice 8-16 weeks old were injected intraperitoneally (IP) with 10 mg/kg of body weight LPS from Salmonella enterica serotype minnesota (Sigma, L2137) dissolved at 1 mg/ml in sterile PBS. When noted, mice were pre-injected with either NAC (150 μg/kg) or saline, 30 min before an IP injection of 10 mg/kg LPS. Mice were health checked twice per day and weighed once a day for up to 5 days, after which any surviving mice were euthanized by CO2 inhalation. Survival curves were analyzed using the log-rank (Mantel-Cox) test.

7. Genome-wide siRNA screen

The RNAi screen was conducted in 384-well format using the Ambion Silencer Mouse Genome siRNA Library (#4391425), which consists of three unique, nonoverlapping, nonpooled siRNAs for each of 17,000 gene targets. siRNA reagents (2 μl, 2 μM) were stamped into 384-well white flat-bottom microplates (Corning, 3570) using a Velocity11 VPrep liquid handling system (Agilent) integrated into a BioCel robotic platform (Agilent) in columns 1–22, leaving columns 23–24 empty for negative (Ambion, Negative control #1) and positive (mouse *Casp4*) controls, respectively. The median value of each plate's negative control column was used to normalize sample wells, and the positive control was used to assess transfection efficiency and assay performance.

Lipofectamine RNAiMAX Transfection Reagent (0.4 μl; Invitrogen) was added in 20 μl serum-free, antibiotic-free media to plate wells using a Thermo Scientific Matrix WellMate and Microplate Stacker. Plates were incubated for 45 min at room temperature to allow for the sufficient formation of siRNA-lipid complexes. Cells were seeded at a density of $1x10^4$ cells per well in 20 μL media containing 20% (vol/vol) FBS without antibiotics. The final concentration of siRNA in each well was 100 nM. Cells were cultured for 48h at 37°C in 5% CO2 before addition of 10 μl of TLR ligand Pam3CSK4 for 5 hours. The medium was then removed, replaced with 15 μl growth media and cell were transfected with 10 μl of LipidA and TransIT-TKO (Mirus) for 24 hour. At the end of the LipidA treatment, 10 μl of supernatant was transferred to a 384 Greiner Bio-one non-binding low volume plate and 10 μl of IL-1α HTRF reagent (Cisbio, 62MIL1APEH) was added and incubated at room temperature overnight. The plates were read on an EnVision plate reader (PerkinElmer). Cell viability was measured by adding 20ul Cell Titer Glo to the original plate and running a luminescence read on the EnVision. The quantified IL-1α signal for each siRNA gene-targeted well was divided by the median of the negative control wells and multiplied by 100 to achieve a negative control normalized value for each well/siRNA. This normalized value was then used to generate a robust z-score by first taking the log of each value and then by subtracting the median and dividing by the mean absolute deviation. The median z-score was then used to rank genes for follow-up.

8. Calculation of mitochondria-related enrichment among screen hits

Enrichment for mitochondria related genes in hit candidates from the genome-wide screen were evaluated using the Mitochondrial Proteomics Database MitoMiner 4.0 (date accessed June 11, 2020)[73]. The 95th percentile of positive regulators from the genome-wide screen were analyzed through the database and assigned Integrated Mitochondrial Protein Index (IMPI) scores. IMPI scores were converted to negative values for non-mitochondrial candidates and kept positive for candidates predicted or assigned as mitochondrial.

9. BMDM RNAi

BMDMs were reverse transfected with siRNAs against screen hit genes using Viromer Green (Lipocalyx, cat# VG-01LB-00). 0.1 μl of Viromer Green transfection reagent pre-mixed with 4.9 μl of Viromer Green Buffer was mixed with 5 μl of siRNAs (0.5 μM). After incubation for 30 min at room temperature, 4 μl were added to each well of a 384-well plate (Falcon, 353962). Next, 4x10^4 BMDMs in 36 μl of complete DMEM were seeded per well for a final siRNA concentration of 25 nM. Plates were incubated at room temperature for 10 min to allow the cells to settle, then at 37°C in a humidified atmosphere with 5% CO2 for 48 hr. Cells were stimulated for time periods as indicated. For measurement of secreted protein level, supernatants were collected and subject to ELISA as described above. All siRNAs were from ThermoFisher with the following siRNA IDs: 102885, 74210 and 174215 for *Nme3*; 185507, 72411 and 74300 for *Nme4*, 184862 and 73403 for *Nme6*, 159999 and 160000 for *Casp4* (*caspase-11*). Non-targeting negative control siRNA was from Dharmacon (NTC5).

10. Inflammasome activation (prime-trigger) assays

Non-canonical inflammasome: 5x10^4 RAW264.7 macrophages seeded in a 96-well plate were primed with 100 nM P3C for 5 hr, media (80 μl) was replaced and cells were triggered by transfecting 1 μM LipidA for 18 hr (20 μl). Transfection mix included 1 μl of 500 μM LipidA and 4 μl TransIT-TKO (Mirus) added to 95 μl optiMEM (Gibco). The same procedure was used for BMDM except 1 μg/ml P3C was used for priming and transfection was done using the RNAiMAX (ThermoFisher) transfection reagent (3 μl for a total of 100 μl). *Canonical inflammasome*: Procedures were as above except 100 ng/ml LPS for 5 hr was used for priming, and 5 mM ATP or 10 μM Nigericin for up to 2 hr was used for triggering, both for RAW264.7 and BMDM. IL-1α and IL-1β expression were measured by ELISA according to manufacturer's instructions (R&D, #DY400, #DY401).

11. Bacterial infection

Infection of RAW264.7 cells and BMDM with *B. cenocepecia* (provided by Dr. David Greenberg, University of Texas Southwestern) at MOI 10 was conducted using the infection and imaging methods described previously[74,75].

12. Cardiolipin exposure measurement

WT and *Nme4*$^{-/-}$ cells were incubated with 250 nM Mitotracker Green FM (Molecular Probes) for 45 min at 37°C, following the manufacturer's instructions. After stimulation, mitochondrial isolations were performed by differential centrifugation as previously

described[18]. Briefly, the macrophages were resuspended in mannitol-sucrose buffer and subjected to nitrogen cavitation (200 psi, 20 min at 4°C). The disruption of cells was followed by differential centrifugation steps to isolate the mitochondria. Nuclei and unlysed cells were separated from the homogenate by centrifugation at 1000g for 10 min at 4°C. The mitochondria were then pelleted from post-nuclear supernatant by centrifugation at 12,000g for 20 min at 4°C. Following isolation, cardiolipin externalization was assessed by mitochondrial Annexin V staining as previously described[76]. Mitochondria were incubated with Annexin V–Alexa Fluor 647 (Invitrogen) for 30 min on ice. Mitochondria were then washed twice with mannitol-sucrose buffer, fixed with 4% paraformaldehyde, and analyzed by flow cytometry on a BD LSR Fortessa.

13. Quantitative PCR

Total RNA was isolated using Direct-zol096 RNA extraction kit (Zymo Research) according to manufacturer's instructions. RNA was reverse transcribed using iScript Reverse Transcription Supermix cDNA synthesis kit (BioRad). qPCR reactions were carried out using either SYBR Green or TaqMan assays (Applied Biosystems) with gene specific primers and FAM-conjugated probes (Life Technologies). PCR reactions were performed and analyzed in a QuantStudio 6 Flex Real Time PCR system (Applied Biosystems).

14. Fluidigm Quantitative PCR

Quantitative PCR was carried out according to the manufacturer's instructions using the BioMark HD system (Fluidigm), with Fluidigm-designed primer sets. Ct values were automatically calculated and exported from the BioMark HD system, then normalized to either *Hprt* or *Actb*.

15. Mitochondrial fractionation

Mitochondrial fractions were isolated from RAW264.7 cells using a mitochondria isolation kit from ThermoFisher (Cat# 89874). WT and *Nme4*$^{-/-}$ RAW264.7 cells ($5x10^6$ cells per sample) were stimulated with 100 ng/ml LPS for 15 minutes. Fractionation was conducted following the manufacturer's protocol. NLRP3 and TRAF6 abundance in the mitochondrial fraction was analyzed by western blot using the following primary antibodies: NLRP3 (AdipoGen, AG-20B-0014-C100), TRAF6 (Abcam, ab33915). TOMM40 (ProteinTech, 66658-1-Ig) and GAPDH (Abcam, ab9485) were used for normalization. Nme4 protein expression in WT and *Nme4*$^{-/-}$ RAW264.7 cells was measured by immunoprecipitation of Nme4 using a rabbit anti-Nme4 antibody (kindly provided by Dr. Marie-Lise Lacombe) with protein A/G beads (ThermoFiscer), then Nme4 was immunoblotted using a mouse anti-Nme4 antibody (Abcam ab228005).

16. Live cell imaging of RAW264.7 macrophages

WT and *Nme4*$^{-/-}$ RAW264.7 cells expressing ASC-GFP were seeded in 96-wells plates at $2.5x10^4$ cell/well and rested overnight. Cells were primed with 100 nM LipidA for 5 hr, stained with Hoechst 33342 for 30 min, and triggered with 10 μM nigericin for 2 hr. During the triggering step, cells were imaged every 5 min at 20X magnification on a Cell Insight CX7 high-content imager (ThermoFisher), with an onstage incubator set to maintain cell

at 37°C and 5% CO_2. At each time point, cells and ASC specks were counted using HCS studio image analysis software (ThermoFisher), and the fraction of cells containing ASC specks was calculated.

17. Pyroptosis and GSDMD cleavage assays

WT and *Nme4*$^{-/-}$ RAW264.7 cells were primed with 100 nM P3C for 5 hr the triggered by LPS electroporation using the Neon Electroporation System (ThermoFisher). 2x10^6 cell were electroporated for 20 ms, 1400V in 2 pulses with 1 μg LPS in resuspension buffer R. After electroporation, cells were resuspended in optiMEM. For pyroptosis assays, 4x10^4 cells were seeded in a black, clear bottom 96-wells plate and stained with 4 μg/ml PI and 1 μg/ml Hoechst. The plate was centrifuged and PI uptake was measured every 15 minutes for 4 hr using a CLARIOstar plate reader (BMG-LabTech). PI uptake was normalized to the number of cells as assessed by Hoechst staining. After the PI assay, the cell supernatant was collected and LDH release was measured according to the manufacturer's instructions (Sigma). For the GSDMD cleavage assay, primed and LPS electroporated cells (or control electroporated cells) were seeded in a 12-well plate at 5x10^5 cells/well for 3 hr. Whole lysates were collected and immunoblotted for GSDMD (Abcam, ab209845).

18. Western blotting

WT and *Nme4*$^{-/-}$ cells were treated with LPS for the indicated times and lysed in the presence of protease and phosphatase inhibitor cocktails (Roche). Cell extracts (20 μg protein) were boiled for 5 min in SDS-PAGE buffer, subjected to 4-12% gradient SDS-PAGE, proteins were transferred and the nitrocellulose membrane was blocked using 5% milk for 1 hr. The primary antibodies used were: phosho-p38 MAPK (Cell-Signaling, #4511), phospho-ERK1/2 (Cell-Signaling, #4370), phospho-NF-κB (Cell-Signaling, #3033), IκB (Cell-Signaling, #4814), phospho-TBK1 (Cell-Signaling, #5483), NLRP3 (Adipogen, AG-20B-0014-C100), Caspase-11 (Cell-Signaling, #14340), TRAF6 (Abcam, ab33915), RhoGDI (Sigma, R3025), pro-IL-1α, pro-IL-1β (R&D). Western blots were incubated with respective HRP-conjugated secondary antibodies (Sigma) and using ECL reagents (Bio-Rad) on the ChemiDoc imager (Bio-Rad). Immunoblot data was analyzed using ImageJ software and data from three replicate experiments were quantified for statistical analysis.

19. ROS assays

ROS measurement at the cell population level was assessed in 1x10^4 RAW264.7 cells seeded per-well of an opaque 384-well plate. The next day the cells were treated with 100 ng/ml LPS and ROS production was measured using the hydrogen peroxide-based ROS-glo assay kit (Promega, G8820), according to the manufacturer's protocol.

Single-cell ROS measurements were conducted in RAW264.7 cells treated with 100 ng/ml LPS for the indicated times and stained with 1 μM MitoSOX (ThermoFisher) for 15 minutes, following two washes with PBS. Cells were then either collected and measured for fluorescence by Fortessa flow cytometer (BD Biosciences) and analyzed on FlowJo, or imaged on the Cell Insight CX7 imager (ThermoFisher) after further staining with Hoechst 33342 (ThermoFisher, R37605). Image analysis on the CX7 was done using the HCS Studio (ThermoFisher) using the spot counting protocol. Spots intensity was analyzed specifically

in the cytoplasm, by segmenting the nuclei based on the Hoechst channel and defining a ring around it.

20. Mitochondrial membrane potential and mitochondrial mass measurements

RAW264.7 cells were treated with 100 ng/ml LPS for the indicated time and stained with 200 nM TMRM or 250 nM MitoTracker Green for 30 min in phenol-free DMEM. Cells were washed twice and fluorescence was detected using a CLARIOstar plate reader (BMG-LabTech).

21. Metabolic analyses

Oxygen consumption rate (OCR) and extracellular acidification rate (ECAR) were examined using the XF96 Seahorse Metabolic Analyzer from Seahorse Biosciences. Briefly, $3x10^4$ RAW264.7 cells or $1x10^5$ BMDM were cultured overnight in complete media. The next day, media was changed to Seahorse XF media and cells were incubated for 1 hr at 37°C without CO_2. Metabolic mitochondrial stress tests were performed according to the manufacturer's protocol. Port injections and times are indicated in the figures. Mitochondrial ATP OCR and maximal respiratory capacity are defined as the percentage of OCR that is oligomycin or antimycin A/rotenone sensitive, respectively. When indicated, 100 ng/ml LPS, 10 mM 2-DG, and/or 250 μM mitoTempo was added during the assay to assess metabolic changes. Where noted, data are represented as percent of control levels calculated as the mean of the basal state. In other assays, BMDM were incubated in complete culture media supplemented with 100 ng/ml of LPS overnight.

Metabolic profile studies were done by Liquid Chromatography Mass Spectrometry (LC-MS). LCMS-grade solvents were used for all metabolomics methods. RAW264.7 cells were seeded at $5x10^5$ in a 6-well plate and treated with 100 ng/ml of LPS for 0, 0.5, 1, 2, 4, 8, 24 hr. The experiment was stopped by removing media, washing with 1 ml of 0.9% sodium chloride and immediately immersing in 0.4 ml of ice-cold methanol for 5 minutes. Next, 0.4 ml of ice-cold water were added and cells were scraped and collected in Eppendorf tubes. 0.4 ml of ice-cold chloroform was added to each sample and samples were shaken for 30 minutes at 4°C then centrifuged at 16,000 g for 20 minutes. 550 μl of the top (aqueous) layer was collected and stored at −80°C. For LC-MS injection, samples were separated using a Sciex ExionLC™ AC system and analyzed using a Sciex 5500 QTRAP® mass spectrometer. The order of injections was randomized. To account for carry over and instrument drift, quality control (QC) and blank injections were distributed throughout the runs.

Metabolites were measured using a previously established ion pairing method with modification[77]. Samples were separated on a Waters Atlantis T3 column (100Å, 3 μm, 3 mm X 100 mm) and eluted with a gradient from 5 mM tributylamine, 5 mM acetic acid in 2% isopropanol, 5% methanol, 93% water (v/v) to 100% isopropanol over 15 minutes. All targets utilized negative mode with two distinct MRM pairs per metabolite. Only relative quantification was performed.

All signals were integrated using MultiQuant® Software 3.0.3. Signals with greater than 50 % missing values or a QC coefficient of variance of greater than 30 % were discarded. Remaining missing values were replaced with the lowest registered signal value. Signals

were normalized using total sum normalization. Initial analysis was performed with multiple MRM signals included for each metabolite when possible. For display and pathway mapping a single MRM signal was used for each metabolite. Univariate t-tests were performed in MarkerView® Software 1.3.1. For all univariate analysis an unpaired t-test was used and a Benjamini-Hochberg correction with a false discovery of 10 % was utilized to correct for multiple comparisons.

22. Cytosolic mtDNA quantification

Cells were seeded at $2x10^6$ in a 6-well plate and 24 hr later were treated with 100 ng/ml of LPS for 2 hr. Cells were collected in PBS and divided into two batches. Total DNA extract was prepared from one batch by suspension in 50 μM NaOH, boiling for 30 min and neutralizing with 50 μl 1M Tris-HCl ph 8. The other batch was suspended in 500 μl solubilization buffer (150 mM NaCl, 50 mM HEPES pH 7.4, and 25 μg/ml digitonin), incubated for 10 min and centrifuged at 980g for 3 min to pellet nuclei. The supernatant, containing the mtDNA, was centrifuged at 17,000g for 10 min to pellet intact mitochondria and any remain debris, and mtDNA was isolated from the supernatant using QIAQuick Nucleotide Removal Columns (Qiagen). Mitochondrial DNA was quantified using RT-PCR from 10 ng DNA and calculated as cytosolic mtDNA relative to whole cell mtDNA.

23. Statistical analysis

Data are presented as means ± standard deviation (± SD) or mean ± standard error mean (± SEM) for Seahorse assays, and are representative of at least two independent experiments. Statistical analysis was performed using GraphPad Prism 7. One-way or two-way ANOVA tests were used when multiple groups were analyzed as indicated in figure legends. Student's t-test was used when two groups were compared.

24. Data visualization

Heatmaps were generated using Morpheus (software.broadinstitute.org/morpheus/) and MeV (mev.tm4.org) analysis and visualization and software.

Supplementary Material

Refer to Web version on PubMed Central for supplementary material.

Acknowledgments

We thank Dr. Marie-Lise Lacombe from INSERM, Centre de Recherche Saint-Antoine, France, for the antibody against Nme4. We thank colleagues in the Laboratory of Immune System Biology for helpful discussions and critical reading of the manuscript. We thank Dr. Danielle A. Sliter (NCI) for protocol advice on mitochondrial DNA quantification, Dr. David Greenberg (UT Southwestern) for provision of *B. cenocepecia* strains and Dr. Lu Chen (NCATS) for assistance with data deposition to PubChem. F.S.S. was supported by the NIH grant R01AI118719. This work was generously supported by the Intramural Research Program of the National Institute of Allergy and Infectious Diseases.

Data availability

Data supporting the findings of this work are available within the paper, its supplementary information and source data files. The genome-wide screen data have been deposited to PubChem BioAssays repository (AID 1508600).

Bibliography

1. Akira S, Uematsu S & Takeuchi O Pathogen recognition and innate immunity. Cell 124, 783–801 (2006). [PubMed: 16497588]
2. Medzhitov R, Preston-Hurlburt P & Janeway CA A human homologue of the Drosophila Toll protein signals activation of adaptive immunity. Nature 388, 394–397 (1997). [PubMed: 9237759]
3. Poltorak A et al. Defective LPS signaling in C3H/HeJ and C57BL/10ScCr mice: mutations in Tlr4 gene. Science 282, 2085–2088 (1998). [PubMed: 9851930]
4. Kayagaki N et al. Non-canonical inflammasome activation targets caspase-11. Nature 479, 117–121 (2011). [PubMed: 22002608]
5. Kayagaki N et al. Noncanonical inflammasome activation by intracellular LPS independent of TLR4. Science 341, 1246–1249 (2013). [PubMed: 23887873]
6. Shi J et al. Inflammatory caspases are innate immune receptors for intracellular LPS. Nature 514, 187–192 (2014). [PubMed: 25119034]
7. Hagar JA, Powell DA, Aachoui Y, Ernst RK & Miao EA Cytoplasmic LPS activates caspase-11: implications in TLR4-independent endotoxic shock. Science 341, 1250–1253 (2013). [PubMed: 24031018]
8. Franchi L, Eigenbrod T, Muñoz-Planillo R & Nuñez G The inflammasome: a caspase-1-activation platform that regulates immune responses and disease pathogenesis. Nat. Immunol 10, 241–247 (2009). [PubMed: 19221555]
9. Schroder K & Tschopp J The inflammasomes. Cell 140, 821–832 (2010). [PubMed: 20303873]
10. Latz E, Xiao TS & Stutz A Activation and regulation of the inflammasomes. Nat. Rev. Immunol 13, 397–411 (2013). [PubMed: 23702978]
11. Malik A & Kanneganti T-D Inflammasome activation and assembly at a glance. J. Cell Sci 130, 3955–3963 (2017). [PubMed: 29196474]
12. Bryant C & Fitzgerald KA Molecular mechanisms involved in inflammasome activation. Trends Cell Biol. 19, 455–464 (2009). [PubMed: 19716304]
13. Mariathasan S et al. Cryopyrin activates the inflammasome in response to toxins and ATP. Nature 440, 228–232 (2006). [PubMed: 16407890]
14. Shimada K et al. Oxidized mitochondrial DNA activates the NLRP3 inflammasome during apoptosis. Immunity 36, 401–414 (2012). [PubMed: 22342844]
15. Allen IC et al. The NLRP3 inflammasome mediates in vivo innate immunity to influenza A virus through recognition of viral RNA. Immunity 30, 556–565 (2009). [PubMed: 19362020]
16. Stutz A et al. NLRP3 inflammasome assembly is regulated by phosphorylation of the pyrin domain. J. Exp. Med 214, 1725–1736 (2017). [PubMed: 28465465]
17. Hornung V et al. Silica crystals and aluminum salts activate the NALP3 inflammasome through phagosomal destabilization. Nat. Immunol 9, 847–856 (2008). [PubMed: 18604214]
18. Iyer SS et al. Mitochondrial cardiolipin is required for Nlrp3 inflammasome activation. Immunity 39, 311–323 (2013). [PubMed: 23954133]
19. Zhou R, Yazdi AS, Menu P & Tschopp J A role for mitochondria in NLRP3 inflammasome activation. Nature 469, 221–225 (2011). [PubMed: 21124315]
20. Subramanian N, Natarajan K, Clatworthy MR, Wang Z & Germain RN The adaptor MAVS promotes NLRP3 mitochondrial localization and inflammasome activation. Cell 153, 348–361 (2013). [PubMed: 23582325]
21. Zhong Z et al. New mitochondrial DNA synthesis enables NLRP3 inflammasome activation. Nature 560, 198–203 (2018). [PubMed: 30046112]

22. Martinon F, Pétrilli V, Mayor A, Tardivel A & Tschopp J Gout-associated uric acid crystals activate the NALP3 inflammasome. Nature 440, 237–241 (2006). [PubMed: 16407889]
23. Lamkanfi M, Kanneganti T-D, Franchi L & Núñez G Caspase-1 inflammasomes in infection and inflammation. J. Leukoc. Biol 82, 220–225 (2007). [PubMed: 17442855]
24. Liu X et al. Inflammasome-activated gasdermin D causes pyroptosis by forming membrane pores. Nature 535, 153–158 (2016). [PubMed: 27383986]
25. Sutterwala FS et al. Critical role for NALP3/CIAS1/Cryopyrin in innate and adaptive immunity through its regulation of caspase-1. Immunity 24, 317–327 (2006). [PubMed: 16546100]
26. Elliott EI et al. Cutting edge: mitochondrial assembly of the NLRP3 inflammasome complex is initiated at priming. J. Immunol 200, 3047–3052 (2018). [PubMed: 29602772]
27. Tannahill GM et al. Succinate is an inflammatory signal that induces IL-1β through HIF-1α. Nature 496, 238–242 (2013). [PubMed: 23535595]
28. Platnich JM et al. Shiga Toxin/Lipopolysaccharide Activates Caspase-4 and Gasdermin D to Trigger Mitochondrial Reactive Oxygen Species Upstream of the NLRP3 Inflammasome. Cell Rep. 25, 1525–1536.e7 (2018). [PubMed: 30404007]
29. Chung I-C et al. Mitochondrial oxidative phosphorylation complex regulates NLRP3 inflammasome activation and predicts patient survival in nasopharyngeal carcinoma. Mol. Cell Proteomics (2019). doi:10.1074/mcp.RA119.001808
30. Everts B et al. TLR-driven early glycolytic reprogramming via the kinases TBK1-IKKε supports the anabolic demands of dendritic cell activation. Nat. Immunol 15, 323–332 (2014). [PubMed: 24562310]
31. Mills EL et al. Succinate dehydrogenase supports metabolic repurposing of mitochondria to drive inflammatory macrophages. Cell 167, 457–470.e13 (2016). [PubMed: 27667687]
32. Baseler WA et al. Autocrine IL-10 functions as a rheostat for M1 macrophage glycolytic commitment by tuning nitric oxide production. Redox Biol 10, 12–23 (2016). [PubMed: 27676159]
33. Cameron AM et al. Inflammatory macrophage dependence on NAD+ salvage is a consequence of reactive oxygen species-mediated DNA damage. Nat. Immunol 20, 420–432 (2019). [PubMed: 30858618]
34. Robb EL et al. Control of mitochondrial superoxide production by reverse electron transport at complex I. J. Biol. Chem 293, 9869–9879 (2018). [PubMed: 29743240]
35. Li N et al. Development of a cell system for siRNA screening of pathogen responses in human and mouse macrophages. Sci. Rep 5, 9559 (2015). [PubMed: 25831078]
36. Marine S, Bahl A, Ferrer M & Buehler E Common seed analysis to identify off-target effects in siRNA screens. J. Biomol. Screen 17, 370–378 (2012). [PubMed: 22086724]
37. Chen C-W et al. Two separate functions of NME3 critical for cell survival underlie a neurodegenerative disorder. Proc. Natl. Acad. Sci. USA 116, 566–574 (2019). [PubMed: 30587587]
38. Tokarska-Schlattner M et al. The nucleoside diphosphate kinase D (NM23-H4) binds the inner mitochondrial membrane with high affinity to cardiolipin and couples nucleotide transfer with respiration. J. Biol. Chem 283, 26198–26207 (2008). [PubMed: 18635542]
39. Boissan M, Schlattner U & Lacombe M-L The NDPK/NME superfamily: state of the art. Lab. Invest 98, 164–174 (2018). [PubMed: 29451272]
40. Tsuiki H et al. A novel human nucleoside diphosphate (NDP) kinase, Nm23-H6, localizes in mitochondria and affects cytokinesis. J. Cell Biochem 76, 254–269 (1999). [PubMed: 10618642]
41. Epand RF, Schlattner U, Wallimann T, Lacombe M-L & Epand RM Novel lipid transfer property of two mitochondrial proteins that bridge the inner and outer membranes. Biophys. J 92, 126–137 (2007). [PubMed: 17028143]
42. Schlattner U et al. Dual function of mitochondrial Nm23-H4 protein in phosphotransfer and intermembrane lipid transfer: a cardiolipin-dependent switch. J. Biol. Chem 288, 111–121 (2013). [PubMed: 23150663]
43. Kagan VE et al. NDPK-D (NM23-H4)-mediated externalization of cardiolipin enables elimination of depolarized mitochondria by mitophagy. Cell Death Differ. 23, 1140–1151 (2016). [PubMed: 26742431]

44. Milon L et al. The human nm23-H4 gene product is a mitochondrial nucleoside diphosphate kinase. J. Biol. Chem 275, 14264–14272 (2000). [PubMed: 10799505]
45. Garcia Fernandez M et al. Early changes in intramitochondrial cardiolipin distribution during apoptosis. Cell Growth Differ 13, 449–455 (2002). [PubMed: 12354754]
46. Zhan X et al. LPS-induced mitochondrial DNA synthesis and release facilitate RAD50-dependent acute lung injury. Signal Transduct. Target. Ther 6, 103 (2021). [PubMed: 33654053]
47. Lauterbach MA et al. Toll-like Receptor Signaling Rewires Macrophage Metabolism and Promotes Histone Acetylation via ATP-Citrate Lyase. Immunity 51, 997–1011.e7 (2019). [PubMed: 31851905]
48. Tan Y & Kagan JC Innate immune signaling organelles display natural and programmable signaling flexibility. Cell 177, 384–398.e11 (2019). [PubMed: 30853218]
49. Palsson-McDermott EM et al. Pyruvate kinase M2 regulates Hif-1α activity and IL-1β induction and is a critical determinant of the warburg effect in LPS-activated macrophages. Cell Metab. 21, 65–80 (2015). [PubMed: 25565206]
50. West AP et al. TLR signalling augments macrophage bactericidal activity through mitochondrial ROS. Nature 472, 476–480 (2011). [PubMed: 21525932]
51. Mills EL, Kelly B & O'Neill LAJ Mitochondria are the powerhouses of immunity. Nat. Immunol 18, 488–498 (2017). [PubMed: 28418387]
52. Wardi J et al. 3-Aminobenzamide Prevents Concanavalin A-Induced Acute Hepatitis by an Anti-inflammatory and Anti-oxidative Mechanism. Dig. Dis. Sci 63, 3382–3397 (2018). [PubMed: 30196390]
53. Zhu X et al. Dual ligand stimulation of RAW 264.7 cells uncovers feedback mechanisms that regulate TLR-mediated gene expression. J. Immunol 177, 4299–4310 (2006). [PubMed: 16982864]
54. Victor VM, Rocha M & De la Fuente M N-acetylcysteine protects mice from lethal endotoxemia by regulating the redox state of immune cells. Free Radic. Res 37, 919–929 (2003). [PubMed: 14669999]
55. Yang Z et al. PARP-1 mediates LPS-induced HMGB1 release by macrophages through regulation of HMGB1 acetylation. J. Immunol 193, 6114–6123 (2014). [PubMed: 25392528]
56. de Mello RO et al. Effect of N-acetylcysteine and fructose-1,6-bisphosphate in the treatment of experimental sepsis. Inflammation 34, 539–550 (2011). [PubMed: 20882329]
57. Liu L et al. Proinflammatory signal suppresses proliferation and shifts macrophage metabolism from Myc-dependent to HIF1α-dependent. Proc. Natl. Acad. Sci. USA 113, 1564–1569 (2016). [PubMed: 26811453]
58. Wang A et al. Specific sequences of infectious challenge lead to secondary hemophagocytic lymphohistiocytosis-like disease in mice. Proc. Natl. Acad. Sci. USA 116, 2200–2209 (2019). [PubMed: 30674681]
59. Zheng Z et al. Enhanced glycolytic metabolism contributes to cardiac dysfunction in polymicrobial sepsis. J. Infect. Dis 215, 1396–1406 (2017). [PubMed: 28368517]
60. Attwood PV & Muimo R The actions of NME1/NDPK-A and NME2/NDPK-B as protein kinases. Lab. Invest 98, 283–290 (2018). [PubMed: 29200201]
61. Xue R et al. Metastasis suppressor NME1 promotes non-homologous end joining of DNA double-strand breaks. DNA Repair (Amst.) 77, 27–35 (2019). [PubMed: 30875636]
62. Wang C-H et al. A shRNA functional screen reveals Nme6 and Nme7 are crucial for embryonic stem cell renewal. Stem Cells 30, 2199–2211 (2012). [PubMed: 22899353]
63. Williams NC & O'Neill LAJ A role for the krebs cycle intermediate citrate in metabolic reprogramming in innate immunity and inflammation. Front. Immunol 9, 141 (2018). [PubMed: 29459863]
64. Haschemi A et al. The sedoheptulose kinase CARKL directs macrophage polarization through control of glucose metabolism. Cell Metab. 15, 813–826 (2012). [PubMed: 22682222]
65. Shen Y et al. Bioenergetic state regulates innate inflammatory responses through the transcriptional co-repressor CtBP. Nat. Commun 8, 624 (2017). [PubMed: 28935892]

66. Holmström KM & Finkel T Cellular mechanisms and physiological consequences of redox-dependent signalling. Nat. Rev. Mol. Cell Biol 15, 411–421 (2014). [PubMed: 24854789]

67. Han W et al. NADPH oxidase limits lipopolysaccharide-induced lung inflammation and injury in mice through reduction-oxidation regulation of NF-κB activity. J. Immunol 190, 4786–4794 (2013). [PubMed: 23530143]

68. Schreck R, Rieber P & Baeuerle PA Reactive oxygen intermediates as apparently widely used messengers in the activation of the NF-kappa B transcription factor and HIV-1. EMBO J. 10, 2247–2258 (1991). [PubMed: 2065663]

69. Li C et al. HIF1α-dependent glycolysis promotes macrophage functional activities in protecting against bacterial and fungal infection. Sci. Rep 8, 3603 (2018). [PubMed: 29483608]

70. Zhong Z et al. NF-κB Restricts Inflammasome Activation via Elimination of Damaged Mitochondria. Cell 164, 896–910 (2016). [PubMed: 26919428]

71. Patoli D et al. Inhibition of mitophagy drives macrophage activation and antibacterial defense during sepsis. J. Clin. Invest 130, 5858–5874 (2020). [PubMed: 32759503]

72. Cong L et al. Multiplex genome engineering using CRISPR/Cas systems. Science 339, 819–823 (2013). [PubMed: 23287718]

73. Smith AC & Robinson AJ MitoMiner v3.1, an update on the mitochondrial proteomics database. Nucleic Acids Res. 44, D1258–61 (2016). [PubMed: 26432830]

74. Miller AH, Vayttaden SJ, Al-Khodor S & Fraser IDC Assay Development for Image-Based Quantification of Intracellular Bacterial Replication and Analysis of the Innate Immune Response to Infection. Assay Drug Dev Technol 13, 515–528 (2015). [PubMed: 26505731]

75. Al-Khodor S et al. Burkholderia cenocepacia J2315 escapes to the cytosol and actively subverts autophagy in human macrophages. Cell Microbiol. 16, 378–395 (2014). [PubMed: 24119232]

76. Chu CT et al. Cardiolipin externalization to the outer mitochondrial membrane acts as an elimination signal for mitophagy in neuronal cells. Nat. Cell Biol 15, 1197–1205 (2013). [PubMed: 24036476]

77. McCloskey D, Gangoiti JA, Palsson BO & Feist AM A pH and solvent optimized reverse-phase ion-paring-LC–MS/MS method that leverages multiple scan-types for targeted absolute quantification of intracellular metabolites. Metabolomics 11, 1338–1350 (2015).

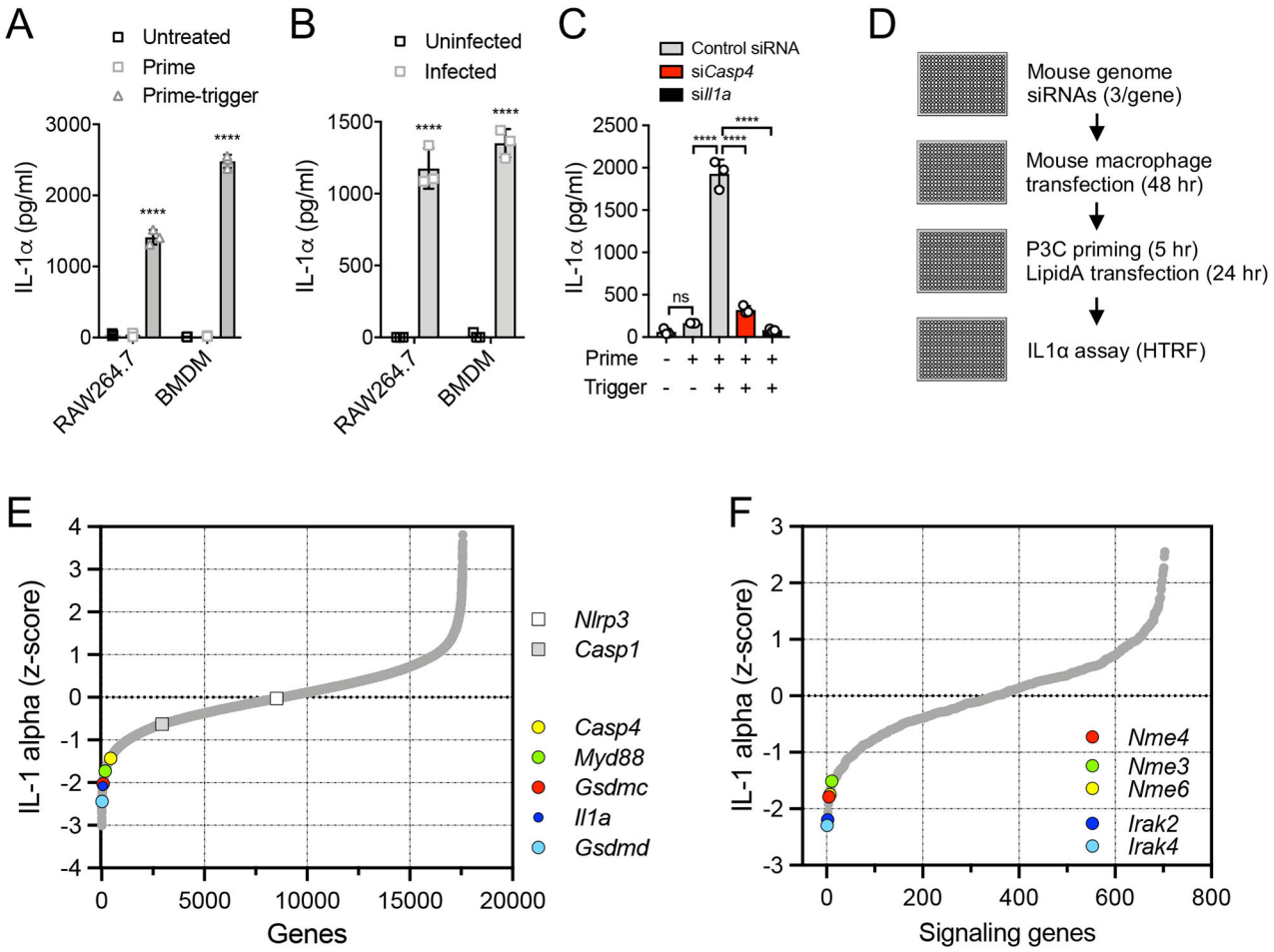

Figure 1: A genome-wide RNAi screen identifies mitochondrial *Nme* genes as positive regulators of the non-canonical inflammasome.

(A) RAW264.7 cells and BMDM were primed with 100 nM or 1 μg/ml P3C (respectively) for 5 hr and triggered by 100 nM LipidA transfection for 18 hr. Secreted IL-1α was measured by ELISA. (B) RAW264.7 cells and BMDM were infected with *B. cenocepecia* (MOI 10) for 18 hr. Secreted IL-1α was measured by ELISA. (C) RAW264.7 cells, transfected with non-targeting control, *Il1a* or *Casp4* siRNA, were primed and triggered as in (A). (D) Arrayed siRNA screen workflow. (E) Phenotypic distribution of the genome-wide screen highlighting known inflammasome components. (F) Phenotypic distribution of a pilot set of signaling genes showing *Irak4* and *Irak2* as a expected priming-dependent hits, and identification of the *Nme* genes as a positive regulators of prime-trigger-induced IL-1α release. (A-C) Data are representative of three independent experiments and expressed as mean ± SD, (n=3); (A, B) Two-Way ANOVA and (C) One-Way ANOVA followed by Tukey's multiple comparison test; (A, B) untreated vs. treated cells; ****$p < 0.0001$.

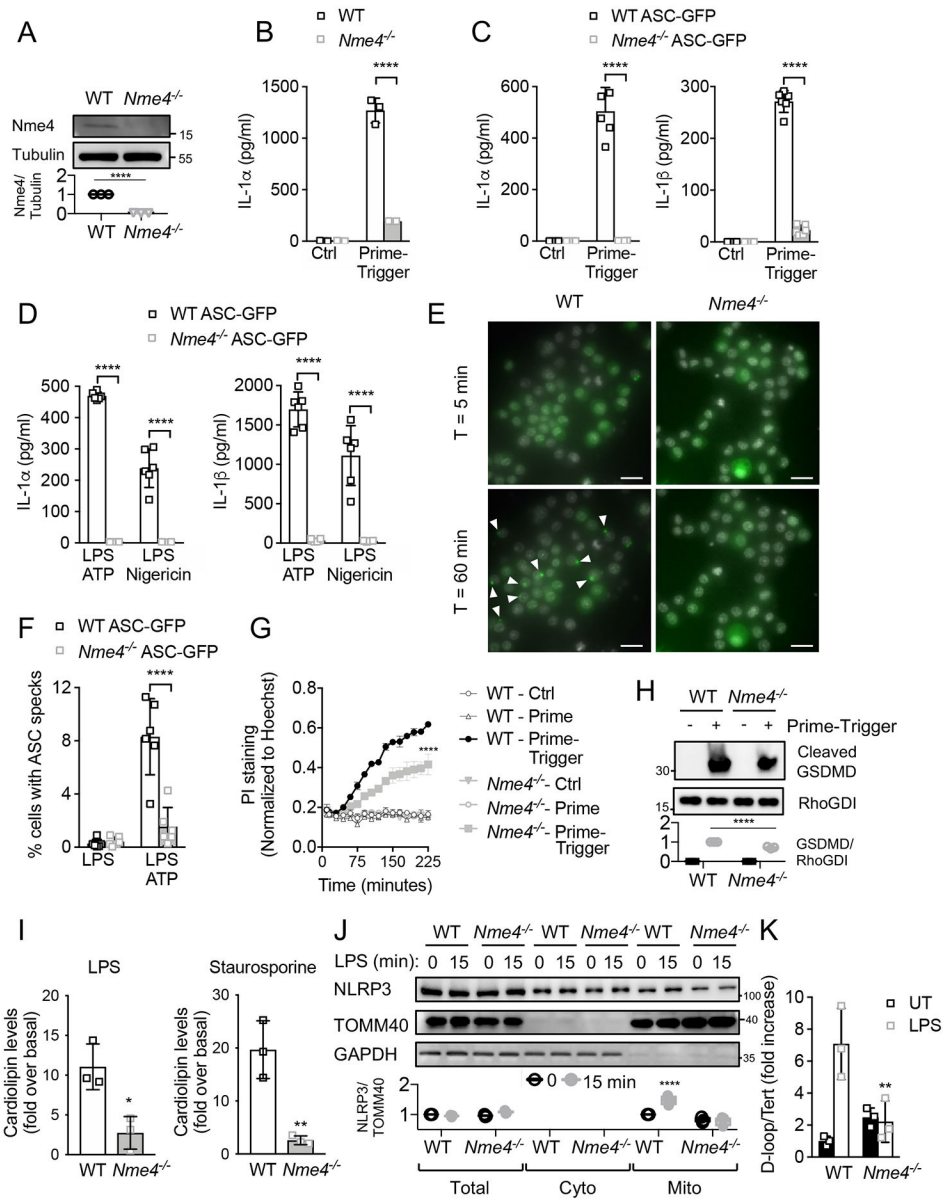

Figure 2: *Nme4* is required for canonical and non-canonical inflammasome responses.

(A) *Nme4* expression analysis from isolated mitochondria of WT or *Nme4*$^{-/-}$ RAW264.7 cells. *Nme4* was pulled down and immunoblotted. Tubulin serves as a pulldown input reference and quantification is plotted. Prime-trigger assays in WT and *Nme4*$^{-/-}$ RAW264.7 cells (B) or WT and *Nme4*$^{-/-}$ RAW264.7 cells stably expressing ASC-GFP (C, D, E, F). IL-1α and IL-1β measurement followed 100 nM P3C priming (6 hr) then (B, C) 100 nM LipidA transfection for 18 hr or (D) 5 mM ATP or 10 μM Nigericin for 30 min. (E, F) 5 mM ATP-induced ASC-GFP speck formation in 100 nM P3C primed ASC-GFP WT or *Nme4*$^{-/-}$ cells. Representative images (ASC specks are highlighted by white arrows); scale bar: 20 μm; (E) and quantification of % speck-positive cells (F). (G, H) WT and *Nme4*$^{-/-}$ RAW264.7 cells were primed for 5 hr with 100 nM P3C then triggered by electroporation of 1μg LPS for 3 hr. PI uptake was measured (4 μg/ml) and normalized to Hoechst staining

(G) while cells were immunoblotted for GSDMD cleavage (H). RhoGDI blot serves as a gel loading reference and blot quantification is plotted. (I) WT or *Nme4*$^{-/-}$ RAW264.7 cells were primed for 4 hr with LPS (100 ng/ml) or Staurosporine (2 μM) and cardiolipin levels in the mitochondrial fraction were measured by FACS analysis of Alexa Fluor 647-Annexin-V staining and normalized to untreated cells. (J) WT or *Nme4*$^{-/-}$ RAW264.7 cells were treated for 15 min with 100 ng/ml LPS and the mitochondrial fraction was isolated and analyzed for NLRP3 recruitment by SDS-PAGE. Relative NLRP3 recrutment to the mitochondrial fraction was plotted. (K) WT or *Nme4*$^{-/-}$ RAW264.7 cells were treated with 100 ng/ml LPS for 2 hr, followed by cytosolic and genomic DNA isolation and quantification by RT-PCR. Results are presented as cytosolic mtDNA vs. nuclear DNA. Data shown are representative of (A-E, G-H, J-K) or pooled from (F, I) at least three independent experiments. (B-D, F-G, I, K) Data expressed as mean ± SD and (I, K) as a fold induction relative to unstimulated cells. (B-D, F-H, J-K) Two-Way ANOVA followed by Sidak's multiple comparison test; **p < 0.01, ****p < 0.0001. (A, I) Welch's two-tailed t-Test; *p < 0.05, **p < 0.01. (C-D, F) n=6 (B, G, I, K) n=3.

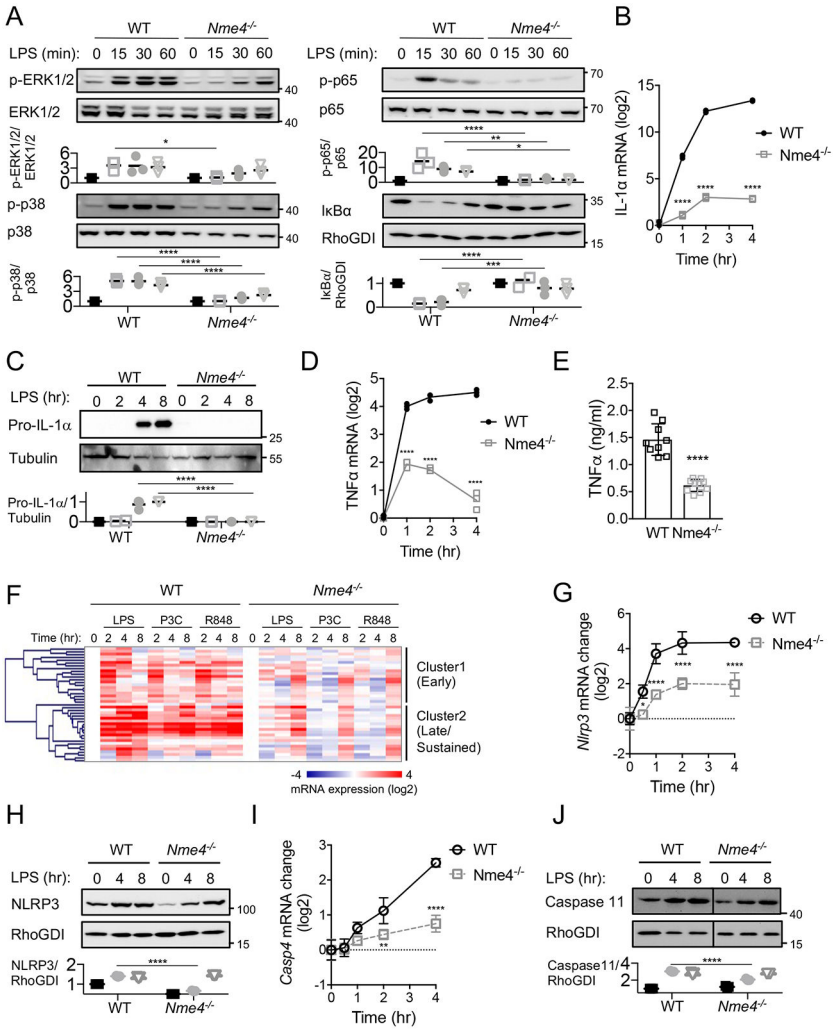

Figure 3: *Nme4* mediates TLR signaling and transcriptional response.

(A) WT or *Nme4*$^{-/-}$ RAW264.7 cells were treated with 100 ng/ml LPS for 0, 15, 30, 45, 60 min and immunoblotted for NF-κB phosphorylation (p-p65), IκB protein levels, ERK phosphorylation and p38 phosphorylation. Total protein levels for p65, ERK1/2, p38 and RhoGDI were assessed as loading controls and relative change quantification is plotted. (B-E) WT or *Nme4*$^{-/-}$ RAW264.7 cells were treated with 100 ng/ml LPS for the indicated times and *Il1a* and *Tnf* mRNA were quantified by qPCR, (C) pro-IL-1α protein expression was analyzed by western blot 0, 2, 4 and 8 hr after stimulation (tubulin blot serves as a gel loading reference) and (E) TNFα secretion at 4 hr was measured by ELISA. (F) Transcriptional response to TLR ligands LPS (100 ng/ml), P3C (1 μg/ml), R848 (5 μg/ml) in WT and *Nme4*$^{-/-}$ cells 0, 2, 4 and 8 hr after stimulation. mRNA levels were assayed by Fluidigm microfluidic RT-PCR and gene expression patterns were analyzed by hierarchical clustering (Pearson uncentered). (G-J) WT or *Nme4*$^{-/-}$ RAW264.7 cells were treated with 100 ng/ml LPS for the indicated times and *Nlrp3* and *casp4* mRNA were quantified by qPCR (G, I). NLRP3 and Caspase11 protein expression was analyzed by western blot 0, 4 and 8 hr after stimulation (RhoGDI serves as a gel loading reference) and quantification is plotted (H, J). Data shown are representative of three (A-E ,G-J) or two (F) independent

experiments, and expressed as mean ± SD (A -E, G-J). (A-D, G-J) Two-Way ANOVA followed by Sidak's multiple comparison test; *p < 0.05, **p < 0.01, ***p < 0.001, ****p < 0.0001, n=3. (E) Welch's two-tailed t-Test; ****p < 0.0001, n=9.

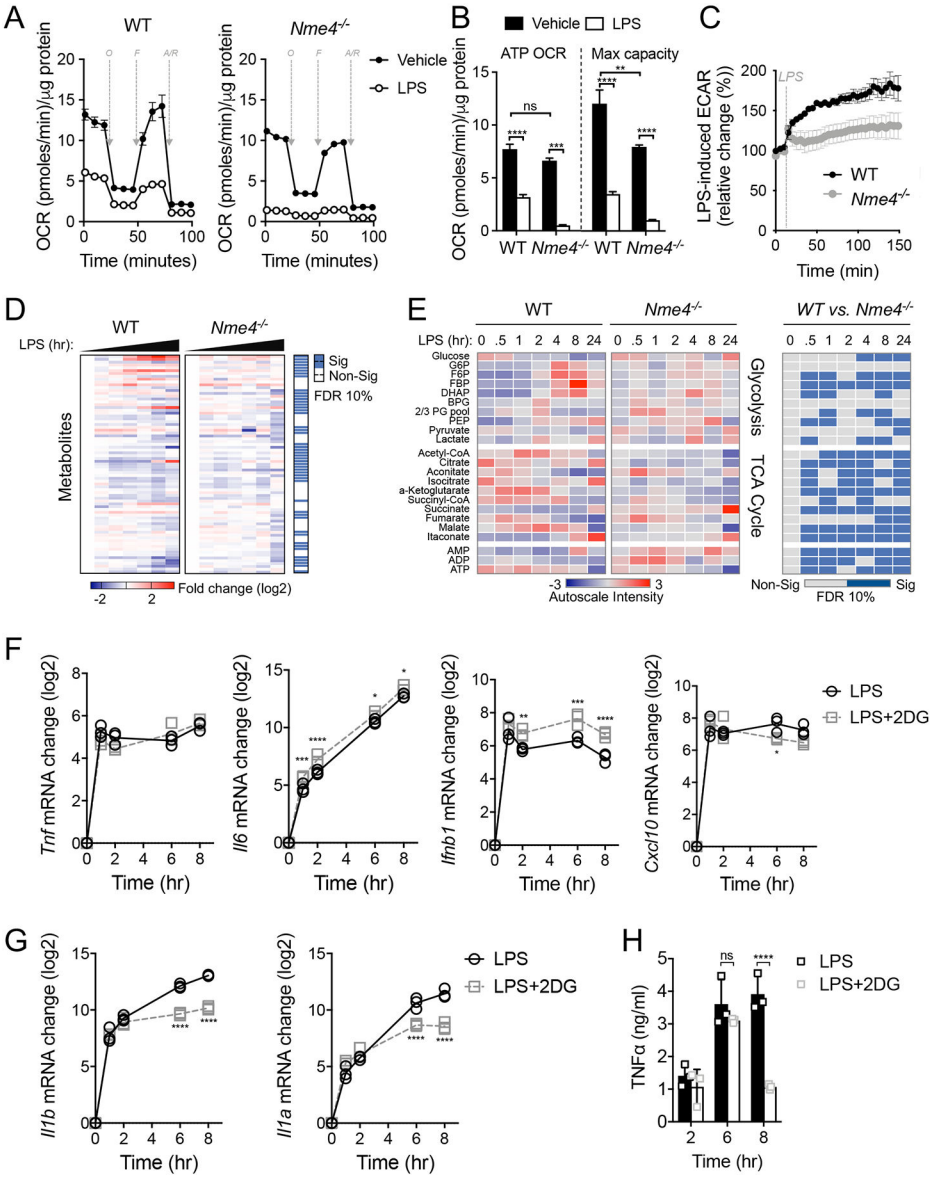

Figure 4: *Nme4* is required for glycolytic commitment induction in LPS-stimulated macrophages.

Representative Seahorse mitochondrial stress test measuring OCR (A) and mitochondrial OCR (B) after 24 hr of 100 ng/ml LPS administration in WT or *Nme4*$^{-/-}$ RAW264.7 cells. O = oligomycin (1 μM), F = FCCP (2 μM), R/AA = Rotenone (0.1 μM) and antimycin A (1 μM). (B) A bar graph showing quantified protein normalized mitochondrial OCR from stress test in (A). (C) Real time ECAR measurement in WT or *Nme4*$^{-/-}$ RAW264.7 cells injected with LPS to a final concentration of 100 ng/ml. (D-E) WT or *Nme4*$^{-/-}$ RAW264.7 cells were treated with 100 ng/ml LPS for 0, 0.5, 1, 2, 4, 8 and 24 hr and the metabolic profile was determined by LC-MS. (D) Log2 fold change on the mean and significance level between groups from an ANOVA2 comparison for time and group variance. (E) Auto-scaled intensity and significance by t-test of the normalized signal from central metabolite signals associated with glycolysis and the TCA cycle over the course of activation. (F-H) WT RAW264.7 cells

were treated with LPS (100 ng/ml) in the presence or absence of 2-DG (5 mM) for the indicated times. (F) *Tnf*, *Il6*, *Ifnb1*, *Cxcl10* and (G) *Il1b* and *Il1a* mRNA were measured by qPCR, and (H) secreted TNFα was measured by ELISA. Data are representative of two (D-E) or three independent experiments (A-C, F-H), and expressed as mean ± SEM (A, C) or mean ± SD (B, F-H). (D-E) Statistical testing was corrected for multiple comparisons using the Benjamini-Hochberg method with a false discovery rate of 10 % equating to p-values of 0.062 for (D), 0.019, 0.047, 0.053, 0.030, 0.067, 0.061 and 0.061 for 0, 0.5, 1, 2, 4, 8 and 24 hr respectively (E). (B, F-H) Two-Way ANOVA followed by Sidak's multiple comparison test; *$p < 0.05$, **$p < 0.01$, ***$p < 0.001$, ****$p < 0.0001$. (A-C, D-E) n=6 (D-F) n=3.

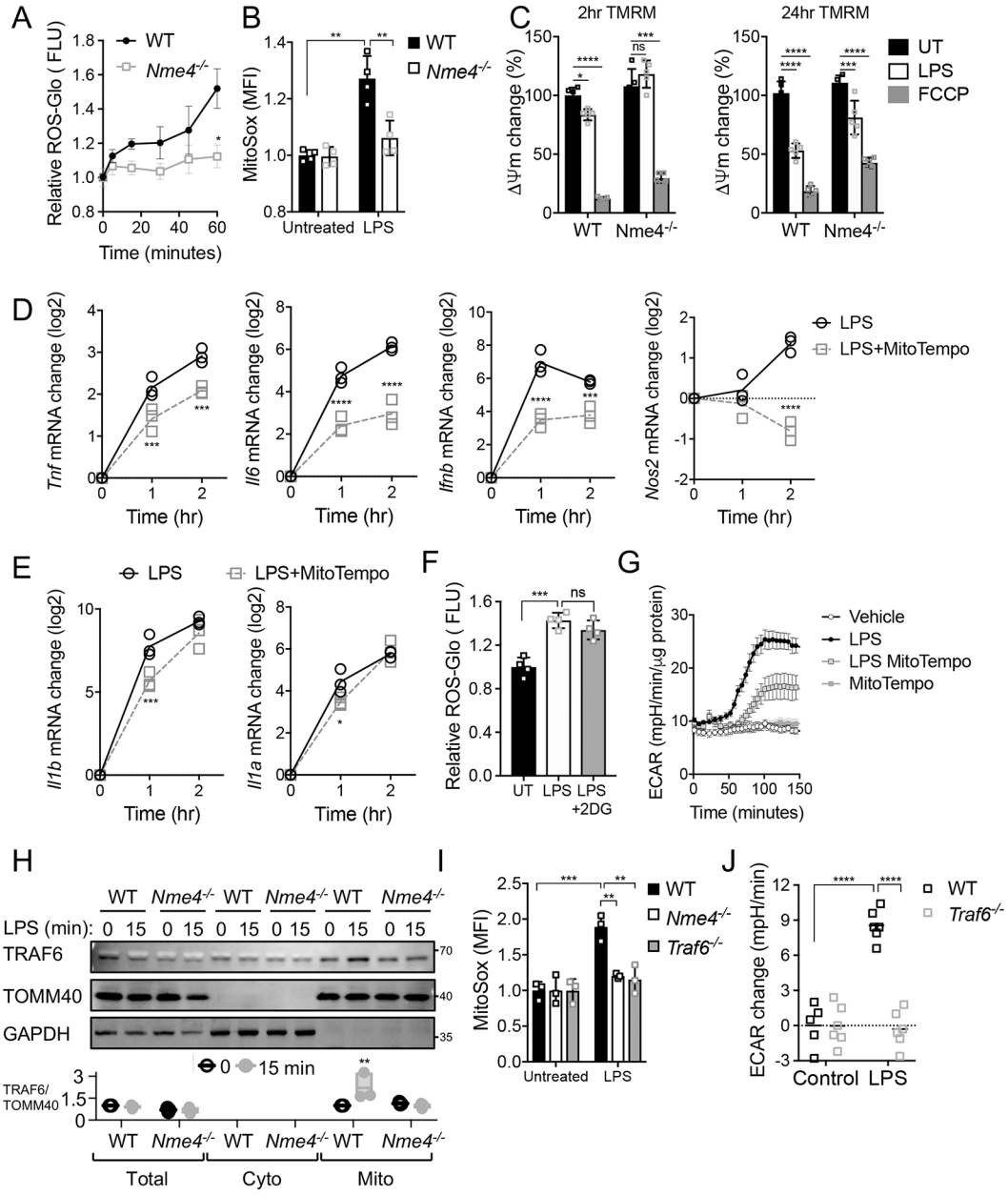

Figure 5: *Nme4* regulates transcription via the TRAF6-*Nme4*-ROS pathway.

(A-B) WT and *Nme4*$^{-/-}$ RAW264.7 cells were treated with 100 ng/ml LPS for up to 1 hr (A) or at 1 hr (B) and early ROS production was measured using a ROS-glo assay (A) or mitoSOX (1 μM) staining and fluorescence imaging by flow (B). (C) Mitochondrial membrane potential change in WT and *Nme4*$^{-/-}$ RAW264.7 cells treated with 100 ng/ml LPS for 2 or 24 hr and stained with 200 nM TMRM (D, E) WT RAW264.7 cells were treated with 100 ng/ml LPS for the indicated times +/− mitoTempo (500 μM) and mRNA levels of the indicated genes were measured by qPCR. (F) Early ROS production in WT RAW264.7 cells treated with 100 ng/ml LPS for 1 hr +/− 5mM 2-DG. (G) Effect of mitochondrial ROS inhibition on the LPS-induced glycolytic switch. Real time ECAR measurement in WT RAW264.7 cells pretreated +/− 500 μM mitoTempo followed by 100

ng/ml LPS. (H) WT or *Nme4*$^{-/-}$ RAW264.7 cells were treated with 100 ng/ml LPS for 15 min and the mitochondrial fraction was isolated and analyzed by SDS-PAGE. Relative TRAF6 recruitment to the mitochondrial fraction is shown. (I) WT, *Nme4*$^{-/-}$ or *Traf6*$^{-/-}$ RAW264.7 cells were treated with 100 ng/ml LPS for 1 hr and ROS production was measured by mitoSOX (1 μM) imaging. (J) ECAR measurement in WT and *Traf6*$^{-/-}$ RAW264.7 cells +/− 15 min treatment with 100 ng/ml LPS. (A-J) Data shown are representative of at least three independent experiments and (A-F, I, J) expressed as mean ± SD, (G) mean ± SEM. (A) Welch's two-tailed t-Test; *$p < 0.05$. (B-E, G-J) Two-Way ANOVA followed by Tukey's multiple comparison test; *$p < 0.05$, **$p < 0.01$, ***$p < 0.001$, ****$p < 0.0001$. (F) One-Way ANOVA followed by Tukey's multiple comparison test; ***$p < 0.001$. (A, D, E, I) n=3, (B,C, F, G) n=4, (J) n=6.

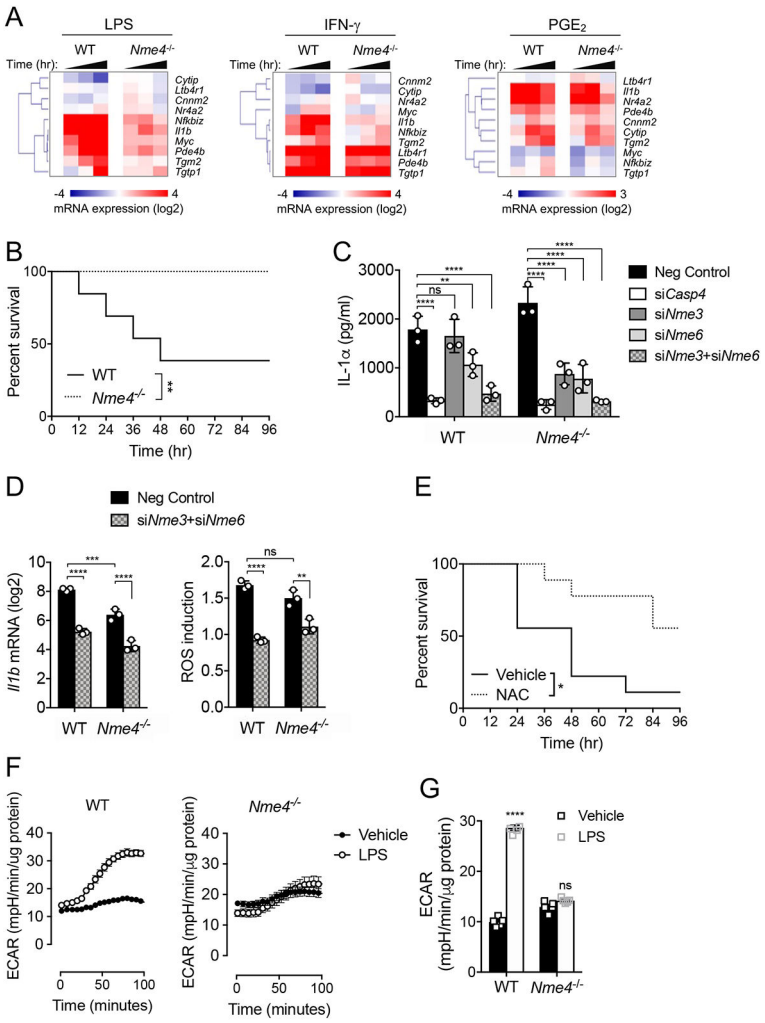

Figure 6: *Nme4* deficient mice are resistant to endotoxic shock.

(A) *Nme4* acts as a mitochondrial checkpoint required to support large-scale gene program. WT or *Nme4*$^{-/-}$ RAW264.7 cells were treated with 100 ng/ml LPS, 5 nM IFNγ or 10 μM PGE_2 for 0, 1, 2, or 4 hr and mRNA levels of the indicated genes were measured by qPCR. (B) Survival of WT or *Nme4*$^{-/-}$ mice after intraperitoneal injection of 10 mg/kg LPS. (C) Primary BMDM from WT or *Nme4*$^{-/-}$ mice were transfected with negative control or *Casp4*, *Nme3* and/or *Nme6* siRNA for 48 hr and then with 1 μg/ml P3C for 6 hr and triggered by 100 nM LipidA transfection for 18 hr. IL-1α secretion was measured by ELISA. (D) Primary BMDM from WT or *Nme4*$^{-/-}$ mice were transfected with negative control or *Nme3* and/or *Nme6* siRNA for 48 hr and then treated with 100 ng/ml LPS for 1 hr. *Il1β* mRNA was quantified by qPCR and early ROS production was measured. (E) Survival of WT mice +/− intraperitoneal injection of 150 mg/kg NAC (30 min) followed by intraperitoneal injection of 10 mg/kg LPS. (F) Real time ECAR measurement in WT and *Nme4*$^{-/-}$ BMDM injected with 100 ng/ml LPS. (G) WT and *Nme4*$^{-/-}$ BMDM were treated with 100 ng/ml LPS for 24 hr followed by a glucose stress test. Quantified ECAR was normalized to protein concentration. Data shown are representative of four (A), five (B), three (C-D, F-G) and two (E) independent experiments, with n=13 WT mice and n=8

Nme4$^{-/-}$ mice (B) and n=9 in each group (E). (B, E) Log-Rank Mantel-Cox Test; * $p < 0.02$, ** $p < 0.01$. (F) Data (n=3 separate wells per group) represent three independent experiments, and expressed as mean ± SEM. (C-D, G) Data Data expressed as mean ± SD and analyzed by Two-Way ANOVA followed by Sidak's multiple comparison test; **$p < 0.01$, ***$p < 0.001$, ****$p < 0.0001$, (C-D) n=3, (G) n=5.

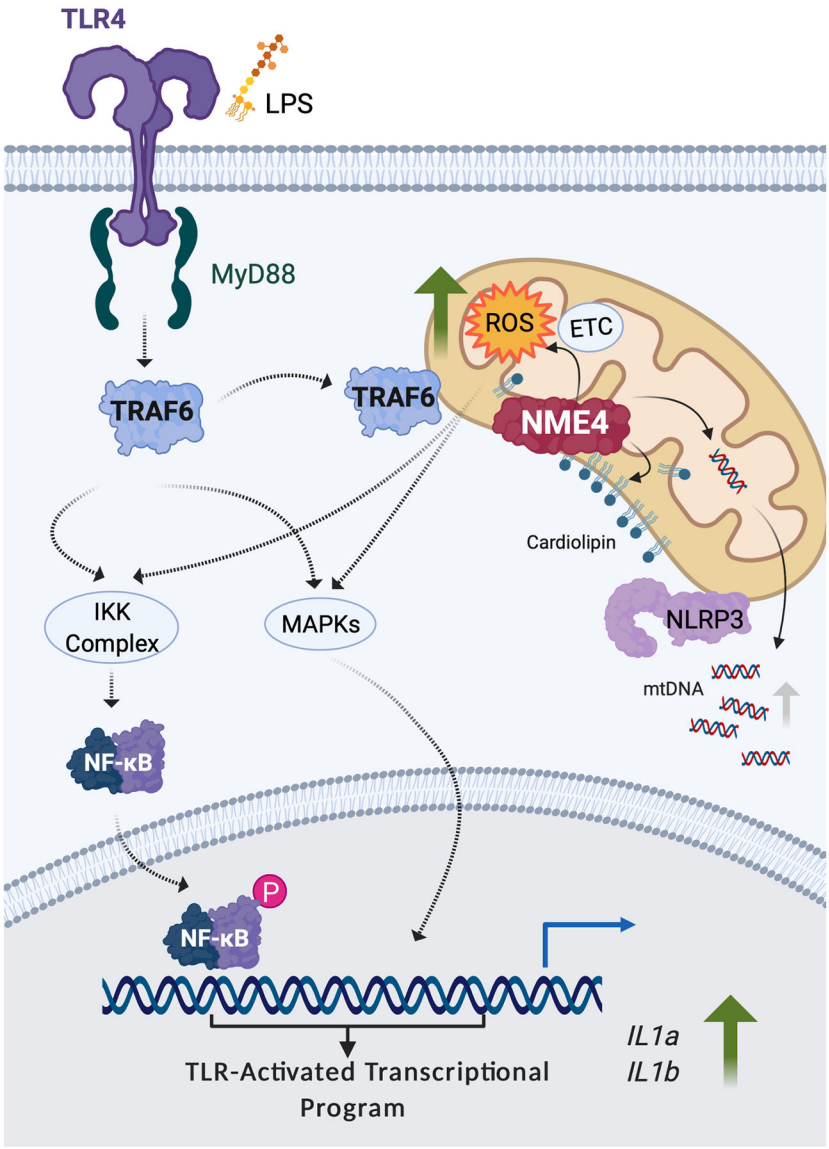

Fig. 7: *Nme4* supports inflammasome activation through multiple roles.

A model illustrating the multiple functions of *Nme4* contributing to inflammasome activation. *Nme4* facilitates recruitment of TRAF6 to the mitochondria and ROS production to support TLR-activated transcription and inflammasome gene priming. Additionally, the lipid transferase function of *Nme4* mediates the cardiolipin exposure required for NLRP3 mitochondrial recruitment and inflammasome licensing, while the nucleoside diphosphate kinase activity of *Nme4* supports TLR-induced mtDNA synthesis. The figure was generated with BioRender.